EXHIBIT 79

Neurobiology of Aging 55 (2017) 99–114

Contents lists available at ScienceDirect

Neurobiology of Aging

journal homepage: www.elsevier.com/locate/neuaging

PTI-125 binds and reverses an altered conformation of filamin A to reduce Alzheimer's disease pathogenesis

Hoau-Yan Wang [a,b,*], Kuo-Chieh Lee [a], Zhe Pei [a], Amber Khan [a,b], Kalindi Bakshi [a], Lindsay H. Burns [c]

[a] Department of Physiology, Pharmacology and Neuroscience, City University of New York School of Medicine, New York, NY, USA
[b] Department of Biology and Neuroscience, Graduate school of the City University of New York, New York, NY, USA
[c] Pain Therapeutics, Inc, Austin, TX, USA

ARTICLE INFO

Article history:
Received 13 December 2016
Received in revised form 6 March 2017
Accepted 9 March 2017
Available online 31 March 2017

Keywords:
Amyloid-beta
Scaffolding protein
Therapeutics
Signal transduction
Tau phosphorylation
Receptor function

ABSTRACT

We show that amyloid-β_{1-42} ($A\beta_{42}$) triggers a conformational change in the scaffolding protein filamin A (FLNA) to induce FLNA associations with α7-nicotinic acetylcholine receptor (α7nAChR) and toll-like receptor 4 (TLR4). These aberrant associations respectively enable $A\beta_{42}$'s toxic signaling via α7nAChR to hyperphosphorylate tau protein, and TLR4 activation to release inflammatory cytokines. PTI-125 is a small molecule that preferentially binds altered FLNA and restores its native conformation, restoring receptor and synaptic activities and reducing its α7nAChR/TLR4 associations and downstream pathologies. Two-month oral PTI-125 administration to triple-transgenic (3xTg) Alzheimer's disease (AD) mice before or after apparent neuropathology and to 8-month wildtypes with milder neuropathologies reduced receptor dysfunctions and improved synaptic plasticity, with some improvements in nesting behavior and spatial and working memory in 3xTg AD mice. PTI-125 also reduced tau hyperphosphorylation, aggregated $A\beta_{42}$ deposition, neurofibrillary tangles, and neuroinflammation. Efficacy in postmortem AD and $A\beta_{42}$-treated age-matched control hippocampal slices was concentration-dependent starting at 1 picomolar (pM) concentration. PTI-125 is the first therapeutic candidate to preferentially bind an altered protein conformation and reverse this proteopathy.

1. Introduction

The most frequent cause of dementia, Alzheimer's disease (AD) is a devastating neurodegenerative disorder with an enormous health care burden and no disease-modifying treatment. The worldwide AD incidence was 46.8 million in 2015 and is estimated to double every 20 years to reach 74.7 million in 2030 and 131 million by 2050 (Prince et al., 2015).

Although amyloid-β, in particular amyloid-β_{1-42} ($A\beta_{42}$), is considered the most causative agent in AD, numerous clinical failures of amyloid-targeting antibodies have challenged this thesis. Potential reasons for these failures include the possible protective effect of amyloid (Hefter et al., 2016) and treating too late in disease progression, as neuropathology precedes symptoms by 10–25 years (Bateman et al., 2012; Trojanowski et al., 2010). However, a prominent toxic effect of soluble $A\beta_{42}$ delivers an additional explanation.

Cognitive impairment and the magnitude of synaptic deficit in AD brain are more highly correlated with soluble $A\beta_{42}$ than with the abundance of amyloid plaques (Haass and Selkoe, 2007; Näslund et al., 2000), which are actually the lysis remnants of degenerated and $A\beta_{42}$-overburdened neurons (D'Andrea and Nagele, 2006). Extensive research has elucidated the role of the α7-nicotinic acetylcholine receptor (α7nAChR) in the toxicity of soluble $A\beta_{42}$ (D'Andrea and Nagele, 2006; Dziewczapolski et al., 2009; Inestrosa et al., 2013; Medeiros et al., 2014; Ni et al., 2013; Ondrejcak et al., 2012). Soluble $A\beta_{42}$ binds and signals via α7nAChR, essentially hijacking this receptor to abnormally activate various kinases (Dineley et al., 2002; Hu et al., 2008; Wang et al., 2003; Zhang et al., 2013) to heighten tau phosphorylation. This hyperphosphorylation of tau alters its normal function and cellular distribution and disrupts axonal/dendritic transport, leading to neurofibrillary lesions, dendritic breakdown, and ultimately neurofibrillary tangles (NFTs) (Wang et al., 2003). Importantly, soluble $A\beta_{42}$ binds α7nAChR with an extraordinarily high (high femtomolar) affinity (Wang et al., 2000a,b), creating substantial competition for antibodies. Amyloid plaques may be more easily bound by antibodies, though this removal may only increase the pool of soluble $A\beta_{42}$ to bind α7nAChR and other, lower affinity targets.

* Corresponding author at: Department of Physiology, Pharmacology and Neuroscience, City University of New York Medical School, 160 Convent Ave., New York, NY 10031, USA. Tel.: +1-212-650-8813; fax: +1-212-650-7726.
E-mail address: hywang@med.cuny.edu (H.-Y. Wang).

0197-4580/$ – see front matter © 2017 Elsevier Inc. All rights reserved.
http://dx.doi.org/10.1016/j.neurobiolaging.2017.03.016

PTI-125 is a novel AD drug candidate that binds the scaffolding protein filamin A (FLNA) to prevent $A\beta_{42}$'s toxic cascade via α7nAChR (Wang et al., 2012). PTI-125's novel mechanism relies on our discovery that $A\beta_{42}$ signaling via α7nAChR requires the association of FLNA with α7nAChR, an otherwise nearly nonexistent interaction (Wang et al., 2012). By binding FLNA, PTI-125 reduces $A\beta_{42}$'s binding affinity for α7nAChR, thereby preventing $A\beta_{42}$'s signaling and further accumulation on α7nAChRs. PTI-125 markedly improved the functioning of α7nAChR, N-methyl-D-aspartate receptor (NMDAR) and insulin receptor (IR) in an intracerebroventricular (ICV) $A\beta_{42}$ infusion mouse model of AD and in human postmortem AD brain, implying some cognitive recovery. PTI-125 even dissociated α7nAChR-bound $A\beta_{42}$ in postmortem AD brain, accomplished by reducing $A\beta_{42}$'s affinity for α7nAChR 1000- to 10,000-fold. In this acute mouse model, PTI-125 also markedly reduced the levels of hyperphosphorylated tau, NFTs and amyloid deposits, indicating slowed disease progression. In a second function, PTI-125 reduced inflammatory cytokine release by reducing an $A\beta_{42}$-induced association of FLNA with TLR4. This combination of functional enhancement, slowed disease progression and reduced neuroinflammation demonstrated by PTI-125 preclinical data is unparalleled by other therapeutic candidates.

We now show that PTI-125 preferentially binds a disease-associated conformation of FLNA. PTI-125 reverses this FLNA proteopathy to prevent its critical role in $A\beta_{42}$'s toxic effects as well as $A\beta_{42}$'s otherwise femtomolar binding to α7nAChR. We demonstrate PTI-125's beneficial effects in triple-transgenic (3xTg) AD mice, starting 2-month oral administration both before and after established neuropathology and in older wild-type mice with substantial Aβ burden. Additionally, using postmortem AD or $A\beta_{42}$-treated age-matched control brain slices, we show efficacy at concentrations as low as 1 picomolar (pM). Importantly, PTI-125 largely restores FLNA to its native conformation in AD brain and in mice but has no effect on native FLNA in controls. This conformation-dependent differentiation suggests a safety advantage despite a ubiquitous target.

2. Materials and methods

2.1. Materials and chemicals

Anti-pY^{960}IRb (44-800G) and $A\beta_{1\text{-}42}$ were obtained from Invitrogen. Anti-PSD-95 (05494), -$A\beta_{42}$ (AB5739), and -NFTs (AB1518) were from Millipore Bioscience Research Reagents. Anti-$pY^{1150/1151}$IRβ (SC-81500), -phosphotyrosine (SC-508), -α7nAChR (SC-65844), -FLNA (SC-7565 [IP], SC-28284, SC-271440), anti–insulin receptor substrate 1 (IRS-1) (SC-515017), -TLR4 (SC-293072), -IRβ (SC-20739, SC-81465), anti–neuronal nitric oxide synthase (nNOS) (SC-5302), -phospholipase C-γ1 (PLCγ1) (SC-7290), -pY^{402}PyK (SC-81512), anti–NMDA receptor subunit 1 (NR1) (SC-1467 [IP], SC-9058 [WB]), anti–NMDA receptor subunit 2A (SC-9056), anti–NMDA receptor subunit 2B (SC-9057), -tau (SC-1995 [IP], SC-58860 [WB]), -γprotein kinase C (SC-166385), -actin (SC-7210), -β-actin (SC-47778), -nitrotyrosine (SC-32757), -Arc (SC-15325 [IP], SC-17839 [WB]), anti–tumor necrosis factorα (TNFα) (SC-8301), anti–Interleukin-6 (IL-6) (SC-7920), anti–Interleukin-1β (IL-1β) (SC-7884) and -tau (SC-1995 [IP], SC-58860 [WB]) were all purchased from Santa Cruz Biotechnology. Anti-pY^{416}Src (#2101) was from Cell Signaling. Anti-$pSer^{202}$tau (AT-8), anti-$pThr^{231}$tau (AT-180), anti-$pThr^{181}$ (AT-270), Reacti-Bind NeutrAvidin high binding capacity coated 96-well plates, covalently conjugated protein A/G-agarose beads, antigen elution buffer and chemiluminescent reagents were purchased from Pierce-Thermo Scientific. Biotinylated anti-IL1β (13-7016-85), anti-TNFα (13-7349-85) and anti–IL-6 (13-7068-85) were purchased from eBioscience. Phosphorstop phosphatase inhibitors (Roche), Complete mini ethylenediaminetetraacetic acid (EDTA) –free protease inhibitor tablet (Roche), and alkaline phosphatase were purchased from Sigma. Aβ-derived peptides were dissolved in 50 mM Tris, pH 9.0 containing 10% dimethyl sulfoxide (DMSO) and stored at −80 °C. All test agents were freshly made according to manufacturer's recommendation. If DMSO was used as the solvent, the highest DMSO concentration in the incubation medium was 1%.

2.2. Postmortem human brain tissue study

This study protocol conformed to the Declaration of Helsinki: Ethical Principles for Biomedical Research Involving Human Beings (the 4th amendment) as reflected in a prior approval by the City College of New York and City University of New York School of Medicine human research committee. The participants had a uniform clinical evaluation that included a medical history, complete neurological examination, cognitive testing including Mini–Mental State Examination and other cognitive tests on episodic memory, semantic memory and language, working memory, perceptual speed, and visuospatial ability as well as psychiatric rating. Based on this information, subjects received AD diagnoses based on National Institute of Neurological and Communicative Disorders and Stroke and the Alzheimer's Disease and Related Disorders Association criteria (McKhann et al., 1984). Postmortem brain tissues of the frontal cortex (FCX) from patients with clinically diagnosed sporadic AD and control tissues from normal, age-matched, and neurologically normal individuals were obtained from the Harvard Brain Tissue Resource Center (HBTRC, Belmont, MA, USA) and UCLA Brain Tissue Resource Center (UBTRC, Los Angeles, CA, USA). Both the HBTRC and UBTRC are supported in part by the National Institute of Health. The postmortem time intervals for collecting these brains were ≤13 hours (mean postmortem intervals for collection of AD and control brain samples were 6.0 ± 0.9 hours and 5.8 ± 0.8 hours, respectively). The cases used in this study have 79.4 ± 4.0 and 79.4 ± 3.8 years of age as well as postmortem intervals of 4.6 ± 0.9 and 4.5 ±1.6 hours for ADs and controls, respectively. Diagnostic neuropathological examination was conducted on fixed sections stained with hematoxylin and eosin stain and with modified Bielschowsky silver staining (Yamamoto and Hirano, 1986) to establish any disease diagnosis according to defined criteria (Hyman and Trojanowski, 1997) and brain tissue from age-matched controls was similarly screened. The presence of both neuritic (amyloid) plaques and NFTs in all AD brains was confirmed by Nissl and Bielschowsky staining and characterized immunohistochemically with anti-$A\beta_{42}$ and -NFT staining in frontal and entorhinal cortex as well as hippocampus as described previously (Wang et al., 2000a). Control tissues exhibited only minimal, localized microscopic neuropathology of AD (0–3 neuritic plaques/10× field and 0–6 NFTs/10× field in hippocampus). One gram blocks from Brodmann areas 10 and/or 46 of FCX were dissected using a band saw from fresh frozen coronal brain sections maintained at −80 °C. All postmortem tissues were identified by an anonymous identification number, and experiments were performed as a best matched pair without knowledge of clinical information.

2.3. Ex vivo incubation of brain slices

For in vitro assessments, postmortem tissues were gradually thawed (from −80 °C to −20 °C), sliced using a chilled McIlwain tissue chopper (200 μm × 200 μm × 3 mm) and suspended in ice-cold oxygenated Kreb's-Ringer solution (K-R), containing 25 mM HEPES, pH 7.4, 118 mM NaCl, 4.8 mM KCl, 1.3 mM $CaCl_2$, 1.2 mM KH_2PO_4, 1.2 mM $MgSO_4$, 25 mM $NaHCO_3$, 10 mM glucose, 100 μM

ascorbic acid, and protease inhibitors (approximately 20 mg/1 mL K-R). Following centrifugation and 2 additional washes with 1 mL ice-cold K-R, brain slices were suspended in 1 mL K-R.

To test the ex vivo effects of PTI-125 on $A\beta_{42}$-incubated control and native AD tissues, PTI-125 (1 pM–1 nM) was added simultaneously with 0.1 μM $A\beta_{42}$. Incubation continued for 1 hour in the dark. The incubation mixture in a total incubation volume of 0.5 mL was aerated for 1 minute every 15 minutes with 95% O_2/5% CO_2. Reactions were terminated by addition of 1.5 mL ice-cold Ca^{2+}-free K-R containing protease and protein phosphatase inhibitors, and slices were collected by a brief centrifugation.

2.4. Assessment of PTI-125 affinity for FLNA

PTI-125's affinity for FLNA was measured in synaptic membranes prepared from postmortem hippocampus of control and AD subjects. Brain tissue was homogenized and processed immediately to prepare synaptosomes (P2 fraction) as described previously (Wang et al., 2003). Synaptosomes (200 μg) prepared from postmortem hippocampus from control and AD subjects were lysed by brief sonication in hypertonic solution (50 mM Tris HCl, pH 7.4, 11.8 mM NaCl, 0.48 mM KCl, 0.13 mM $CaCl_2$, 0.12 mM KH_2PO_4, 0.13 mM $MgSO_4$, 2.5 mM $NaHCO_3$, cocktail of protease, and protein phosphatase inhibitors) and used as the tissue source to determine PTI-125 affinity for FLNA by displacement radioligand binding assay in the presence of 16 concentrations of PTI-125. In this assay, nonspecific binding was defined with 1 μM naltrexone. Briefly, a displacement curve was generated for the inhibition of [^{3}H]naloxone (0.5 nM) binding by PTI-125 to the enriched synaptic membranes from hippocampus from control and AD subjects. A nonlinear curve-fit analysis was performed using competition equation that assumed 2 saturable sites for the PTI-125 curve comprised of 16 concentrations ranging from 100 fM–1 μM using GraphPad Prism software. Six best matched control-AD pairs were included in the analysis.

In a separate experiment series, PTI-125's affinity for FLNA was determined in immunopurified FLNA using [C^{14}]PTI-125 (57.7 Ci/mmol). Briefly, synaptosomes were prepared from postmortem hippocampus of control and AD subjects as described above. The resultant synaptosomes were sonicated in 150 μL immunoprecipitation buffer on ice and solubilized with 0.5% NP40/0.2% Na cholate/0.5% digitonin at 4 °C for 1 hour with end-over-end rotation. Following centrifugation to remove insoluble debris, the protein concentrations of the resultant brain lysates were determined by the Bradford method. One milligram of brain lysates were immunoprecipitated with 5 μg immobilized anti-FLNA on protein A/G-conjugated agarose beads in a total of 5 mL overnight at 4 °C. The immunocomplexes were collected by centrifugation and washed 3 times with phosphate-buffered saline (PBS) containing 0.05% NP-40 and 0.02% Na cholate. The FLNA protein levels were estimated by the Bradford method by subtracting protein A/G-agarose determined by the Bradford method. In this assay, nonspecific binding was defined with 100 μM PTI-125. Briefly, a binding curve was generated by incubation of 0.1 μg immunopurified FLNA from control or AD hippocampus with 50 fM–500 nM at 30 °C for 30 minutes. A nonlinear curve-fit analysis was performed using an equation that assumed 2 saturable sites for the PTI-125 curve comprised of 16 concentrations ranging from 50 fM–500 nM using GraphPad Prism software. Six best matched control-AD pairs were included in the analysis.

2.5. Isoelectric point assessment

To purify FLNA, synaptosomes were prepared from postmortem hippocampi of well-matched control and AD pairs that were incubated with 1 nM PTI-125 ex vivo as described above. To ascertain whether PTI-125 exerts its effects on conformation by binding a specific site on FLNA as previously identified (Wang et al., 2008), control and AD hippocampal synaptosomes were incubated with either 1 nM PTI-125 alone or 1 nM PTI-125 + 10 μM VAKGL ex vivo for 1 hour as described above. Synaptosomes (200 μg) were then sonicated for 10 seconds on ice in 200 μL of modified hypotonic solution (50 mM Tris HCl, pH 8.0, 11.8 mM NaCl, 0.48 mM KCl, 0.13 mM $CaCl_2$, 0.13 mM $MgSO_4$, 2.5 mM $NaHCO_3$, cocktail of protease inhibitors) and treated with 100 μg/mL of alkaline phosphatase at 30 °C for 30 minutes. The reaction was terminated by addition of 100 μM sodium vanadate and 5 mM NaF with cocktail of protein phosphatase inhibitors and solubilized using 0.5% digitonin/0.2% sodium cholate/0.5% NP-40 at 4 °C with end-over-end rotation for 1 hour. Following centrifugation to remove insoluble debris, the obtained lysate was treated with 1% sodium dodecyl sulfate (SDS) for 1 minute to dissociate the FLNA-associated proteins, diluted 10-fold with immunoprecipitation buffer, and imunopurified with immobilized anti-FLNA. The resultant FLNA was eluted using 200 μL antigen-elution buffer (Thermo), neutralized immediately with 100 mM Tris HCl (pH 9.0), diluted to 500 μL with 50 mM Tris HCl, pH 7.5, and passed through a 100 kD cut-off filter to remove low-molecular weight FLNA fragments. Once purified, the FLNA was suspended in 100 μL isoelectric focusing sample buffer. Samples (50 μL) were loaded onto pH 3–10 isoelectric focusing gels and the proteins were fractionated (100 V for 1 hour, 200 V for 1 hour, and 500 V for 30 minutes). The separated proteins were then electrophoretically transferred to nitrocellulose membranes. FLNA was identified by Western blotting with anti-FLNA.

2.6. The assessment of residual PTI-125 using [C^{14}]PTI-125 binding

The levels of residual PTI-125 in brains of treated mice were estimated using [C^{14}]PTI-125 binding. Synaptosomes were prepared from ~10 mg prefrontal cortices from ICV $A\beta_{42}$ infused mice treated twice daily with vehicle or PTI-125 (10 mg/kg) as well as 4- and 8-month-old mice treated for 2 months orally (30 mg/kg/d of PTI-125 HCl). Tissues were lysed by brief sonication in hypertonic solutions to obtain synaptosomes. The resultant synaptic membranes were washed 3 times in 2 mL ice-cold binding buffer (50 mM Tris HCl, pH 7.4, 100 mM NaCl, protease, and protein phosphatase inhibitors). To assess [C^{14}]PTI-125 binding, 50 μg of synaptic membranes were incubated with 1 nM [C^{14}]PTI-125 (57.7 Ci/mmol) in 250 μL at 30 °C for 30 minutes. The synaptic membranes were collected by filtration on GF/C filter under vacuum. Following 3 washes with ice-cold binding buffer, the resultant filters were air dried and counted by scintillation spectrometry. The data are expressed as pg of PTI-125 per mg of synaptic membranes.

2.7. In vivo oral administration of PTI-125

Four- and 8-month-old male and female E129 mice (30–35 g) from Taconic (Germantown, NY, USA) and 3xTg AD mice (containing 3 mutations: APP Swedish, MAPT P301L, and PSEN1 M146V) of stock supplied by Dr. Frank LaFerla (Oddo et al., 2003) were maintained on a 12-hour light/dark cycle with free access to food and water. All animal procedures comply with the National Institutes of Health Guide for Care Use of Laboratory Animals and were approved by the City College of New York Animal Care and Use Committee.

Mice were housed individually for a week to assess the daily intake of water that had been sweetened with 0.25 g sucralose/100 mL purified water. The average daily water intake was found to be approximately 5 mL.

To assess the effect of in vivo PTI-125, mice received 30 mg/kg/d of PTI-125 HCl (22 mg/kg/d free base equivalent) orally via drinking water (18 mg PTI-125 HCl/100 mL purified water sweetened with

0.25 g sucralose) for 2 months. Mice were sacrificed by decapitation. Brain regions such as FCX and hippocampus from one half of the brain were homogenized and processed immediately after harvesting to obtain synaptosomes (P2 fraction) as described previously (Wang et al., 2003) for neuropharmacological assessments. Synaptosomes were washed twice and suspended in 2 mL ice-cold oxygenated K-R: 25 mM HEPES, pH 7.4; 118 mM NaCl, 4.8 mM KCl, 25 mM $NaHCO_3$, 1.3 mM $CaCl_2$, 1.2 mM $MgSO_4$, 1.2 mM KH_2PO_4, 10 mM glucose, 100 μM ascorbic acid, mixture of protease, and protein phosphatase inhibitors (Roche Diagnostics) that had been aerated for 10 minutes with 95% O_2/5% CO_2. The protein concentration was determined using the Bradford method (Bio-Rad). The other brain halves were immersion-fixed in cold 0.15 M phosphate-buffered 10% formalin, pH 7.4, and processed for immunohistochemical determinations of intraneuronal $A\beta_{42}$ aggregates/plaques and NFTs as well as morphological integrity.

2.8. Assessment of FLNA–α7nAChR, FLNA–TLR4 and $A\beta_{42}$–α7nAChR associations by coimmunoprecipitation

These assessments used previously (Wang et al., 2012) described coimmunoprecipitation methods. Two-hundred mg of synaptosomes from either postmortem brain slices or prefrontal cortex or hippocampus of treated mice were pelleted by centrifugation, solubilized by brief sonication in 250 mL of immunoprecipitation buffer (25 mM HEPES, pH 7.5; 200 mM NaCl, 1 mM EDTA, cocktail of protease, and protein phosphatase inhibitors) and incubated at 4 °C with end-to-end shaking for 1 hour. Following dilution with 750 mL of ice-cold immunoprecipitation buffer and centrifugation (4 °C) to remove insoluble debris, the FLNA–α7nAChR/TLR4 and $A\beta_{42}$–α7nAChR complexes in the lysate were isolated by immunoprecipitation with 16-hour incubation at 4 °C with respective rabbit anti-FLNA (1 mg) and anti-$A\beta_{42}$ antibodies (1 mg) immobilized on protein A-conjugated agarose beads. The resultant immunocomplexes were pelleted by centrifugation at 4 °C. After 3 washes with 1 mL of ice-cold PBS (pH 7.2) and centrifugation, the isolated FLNA–α7nAChR/TLR4 and $A\beta_{42}$–α7nAChR complexes were solubilized by boiling for 5 minutes in 100 mL of SDS-polyacrylamide gel electrophoresis (PAGE) sample preparation buffer (62.5 mM Tris-HCl, pH 6.8; 10% glycerol, 2% SDS; 5% 2-mercaptoethanol, 0.1% bromophenol blue). The content of α7nAChRs/TLR4s in 50% of the anti-FLNA and α7nAChRs in 50% of the anti-$A\beta_{42}$ immunoprecipitate was determined by Western blotting with monoclonal anti-α7nAChR or -TLR4 antibodies. The FLNA–α7nAChR/TLR4 complex blots were stripped and reprobed with monoclonal anti-FLNA to validate equal immunoprecipitation efficiency and loading. To determine $A\beta_{42}$–α7nAChR complex levels, immobilized rabbit anti-actin (1 μg) protein A-conjugated agarose was added together with anti-$A\beta_{42}$ in the coimmunoprecipitation process. Immunoblotting with monoclonal anti-β-actin was used to determine the content of β-actin in resultant immunoprecipitates to illustrate even immunoprecipitation efficiency and loading.

2.9. Tau phosphorylation and nitration

Using an established method (Wang et al., 2003, 2010), tau proteins in synaptosomes from $A\beta_{42}$-incubated hippocampal slices from control subjects with and without 1 pM-1 nM PTI-125 were immunoprecipitated with immobilized anti-tau (SC-65865), which does not discriminate between phosphorylation states. The levels of phosphorylated tau ($pSer^{202}$tau, $pThr^{231}$tau and $pThr^{181}$tau), nitrated tau (nYtau) as well as total tau precipitated (loading controls) were assessed by Western blotting using antibodies specific to each individual phosphoepitope, anti-nitrotyrosine, and anti-tau, respectively.

2.10. NMDAR and IR signaling assessments

NMDAR and IR signaling were assessed in low Mg^{2+} Kreb's-Ringer (LMKR): 25 mM HEPES, pH 7.4, 118 mM NaCl, 4.8 mM KCl, 1.3 mM $CaCl_2$, 1.2 mM KH_2PO_4, 0.3 mM $MgSO_4$, 25 mM $NaHCO_3$, 10 mM glucose, 100 μM ascorbic acid and protease inhibitors, and K-R, respectively. Slices were aerated with 95% CO2/5% O_2 every 15 minutes for 1 minute. To assess the PTI-125 effect, postmortem hippocampal slices were exposed to PTI-125 (1 pM–1 nM) at 37 °C for 30 minutes prior to addition of NMDA/glycine or insulin. NMDAR activation and signaling were initiated by incubation of ~10 mg of ex vivo treated brain slices with either LMKR (basal) or LMKR containing 10 μM NMDA and 1 μM glycine at 37 °C for 30 minutes. For initiation of IR activation and signaling, ~10 mg of ex vivo treated postmortem human hippocampal slices or in vivo treated mouse prefrontal cortical slices were incubated with either K-R (basal) or K-R containing 1 nM insulin at 37 °C for 30 minutes. The incubation mixtures were aerated with 95% O_2/5% CO_2 every 10 minutes for 1 minute. Ligand stimulation was terminated by the addition of 1 mL ice-cold Ca^{2+}-free K-R containing 0.5 mM aminopolycarboxylic acid (EGTA) and 0.1 mM EDTA with protease and protein phosphatase inhibitors. Slices were harvested by a brief centrifugation and homogenized in 250 μL ice-cold immunoprecipitation buffer. The homogenates were centrifuged at 1000 × g for 5 minutes (4 °C) and the supernatant (postmitochondrial fraction) sonicated for 10 seconds (5 × 2 seconds) on ice. The proteins were solubilized in 0.5% digitonin, 0.2% sodium cholate, and 0.5% NP-40 for 60 minutes at 4 °C with end-over-end rotation. The resultant lysates were cleared by centrifugation at 50,000 × g for 5 minutes and diluted with 0.75 mL immunoprecipitation buffer. Protein concentrations were measured by the Bradford method (Bio-Rad).

To determine NMDAR signaling and the NMDAR association with PSD-95, the levels of NMDAR subunits, PSD-95 and NMDAR-associated signaling molecules were measured in anti-NR1 immunoprecipitates. Brain slice lysates (200 μg) were immunoprecipitated overnight at 4 °C with 2 μg of immobilized anti-NR1 onto covalently conjugated protein A/G-agarose beads (Pierce ENDOGEN). Anti-NR1 immunoprecipitates were incubated with 75 μL antigen elution buffer (Pierce ENDOGEN) and 2% SDS for 2 minutes on ice, centrifuged to remove antibody-protein A-agarose complexes and neutralized immediately with 10 μL 1.5 M Tris buffer, pH 8.8 followed by addition of 15 μL 6 × PAGE sample buffer and boiling for 5 minutes. Half of the obtained eluates (50 μL) were then size fractionated on 7.5% SDS-PAGE. Proteins were transferred to nitrocellulose membrane and the levels of PSD-95, and signaling proteins were measured using Western blotting with specific antibodies for PSD-95, nNOS, phospholipase C-γ1, γprotein kinase C, pY^{402}PyK2, and pY^{416}Src. Blots were stripped and reprobed with anti-NR1 to assess loading.

To determine IR activation and signaling, the levels of $pY^{1150/1151}$- and pY^{960}-IRs as well as IRS-1 recruited to IR were measured in anti-IRβ immunoprecipitates following incubation of brain slices with 1 nM insulin in K-R for 30 minutes. These experiments followed the above procedures for assessing NMDAR signaling, but immunoprecipitated with immobilized anti-IRβ–protein A/G-agarose beads and detected levels of activated IR ($pY^{1150/1151}$ and pY^{960}) and recruited IRS-1 using Western blotting with antibodies for $pY^{1150/1151}$-IRβ, pY^{972}-IRβ or IRS-1. Blots were stripped and reprobed with anti-IRβ to assess loading.

2.11. Assessment of NMDAR activation induced Arc expression

To determine the effect of PTI-125 on NMDAR activation-induced Arc expression, ~10 mg of ex vivo treated postmortem human hippocampal slices or in vivo treated mouse prefrontal

cortical slices were incubated at 37 °C with LMKR for 30 minutes, 10 μM NMDA/1 μM glycine for 10 minutes followed by LMKR for 20 minutes, in a total incubation volume of 200 μL. Following a 30-minute incubation, protein phosphatase inhibitors were added, and the reaction mixture diluted 5-fold with ice-cold Ca^{2+}-LMKR and placed on ice for 5 minutes. Brain slices were collected after brief centrifugation and sonicated for 10 seconds (5 × 2 seconds) on ice in 200 μL of ice-cold immunoprecipitation buffer containing protease and protein phosphatase inhibitors. The homogenates were centrifuged at 1000g for 5 minutes to yield crude post-mitochondrial fractions. The resultant supernatants were solubilized by addition of 0.5% digitonin/0.2% Na cholate/0.5% NP-40 at 4 °C with end-over-end rotation for 1 hour. Following centrifugation to remove insoluble debris, the protein concentrations of the resultant brain lysates were determined by the Bradford method. Brain lysates (200 μg) were immunoprecipitated with 1 μg immobilized anti-Arc and -actin on protein A/G-conjugated agarose beads (serving as immunoprecipitation/loading control) overnight at 4 °C. The immunocomplexes were collected by centrifugation and washed 3 times with PBS containing 0.05% NP-40 and 0.02% sodium cholate and then solubilized by boiling for 5 minutes in 1 × SDS-PAGE sample preparation buffer. Following centrifugation to remove protein A/G-conjugated agarose beads in the solubilized immunoprecipitates, 50% of the resulting supernatant containing Arc, actin, and their associated proteins were size-fractionated by SDS-PAGE.

2.12. Assessment of cytokine levels in mice

Parietal cortices (~10 mg) from vehicle- and PTI-125-treated mice were thawed slowly (−80 °C to −20 °C to −4 °C), homogenized in 100 μL ice-cold homogenization medium (25 mM HEPES, pH 7.5; 50 mM NaCl, mixture of protease and protein phosphatase inhibitors) by sonication and then solubilized with 0.5% NP-40, 0.2% sodium cholate, and 0.5% digitonin at 4 °C for 1 hour with end-over-end shaking. Following centrifugation, lysates were diluted with 500 μL to a total volume 600 μL.

To determine cytokine levels in the lysates, 0.5 μg/well biotinylated mouse monoclonal anti-TNFα, -IL-6, and -IL-1β were coated onto streptavidin-coated plates (Reacti-Bind NeutrAvidin high binding capacity coated 96-well plate). Plates were washed 3 times with ice-cold 50 mM Tris HCl (pH 7.4) and incubated at 30 °C with 100 μL of lysate for 1 hour. Plates were washed 3 times with ice-cold 50 mM Tris HCl (pH 7.4) and incubated at 30 °C with 0.5 mg/well unconjugated rabbit anti-TNFα, -IL-6, and -IL-1β for 1 hour. After 2 washes with 50 mM Tris HCl (pH 7.4), each well was incubated in 0.5 mg/well fluorescein isothiocyanate-conjugated anti-rabbit immunoglobulin G (human and mouse absorbed) for 1 hour at 30 °C. Plates were washed 3 times with 200 μL ice-cold Tris HCl, and the residual fluorescein isothiocyanate signals were determined by a multimode plate reader (DTX880, Beckman). Each lysate was surveyed twice.

2.13. Immunohistochemical studies of mice

Quantitative immunohistochemistry on consecutive 8-μm sections containing prefrontal cortex and entorhinal cortex/hippocampus was used to determine the levels of $A\beta_{42}$ aggregates/plaques and neurofibrillary pathology (NFT and paired helical filament [PHF] immunoreactivity) using single labeling immunohistochemistry as described previously (D'Andrea et al., 2001; Nagele et al., 2002; Wang et al., 2010). One section was immunostained with anti-NFT or -PHF. The next (consecutive) section (often containing the same neuron) was immunostained with anti-$A\beta_{42}$ antibodies to measure relative levels of accumulated $A\beta_{42}$ peptide in neurons. The relative $A\beta_{42}$ accumulation was compared among different cell types using a computer-assisted image analysis as described previously (Wang et al., 2000a,b). Brain tissues were fixed at 4 °C in 0.15 M phosphate-buffered 10% formalin, pH 7.4 for 2 weeks, paraffin embedded, serially sectioned at 5 mm, and processed for brightfield. The $A\beta_{42}$ immunoreactivity was absent when preabsorbing anti-$A\beta_{42}$ with $A\beta_{42}$ but not with $A\beta_{42\text{-}1}$. Specimens were examined using a Nikon FXA microscope with a Princeton Instruments charge coupled device camera and recorded digitally. Relative intensities of the NFT/PHF and $A\beta_{42}$ immunoreactivity were measured and compared among similar and different cell types using Image Pro Plus and Metamorph software. The correlations between the amounts of NFT/PHF immunoreactivity and $A\beta_{42}$-positive accumulation within mature neurons were also determined.

2.14. Assessing spatial memory with Y-maze

The effects of PTI-125 on hippocampus-dependent spatial memory performance were assessed using Y-maze with extra-maze visual cues around maze as previously described (Wesierska et al., 2005). All mice were transported to the behavioral testing room in their home cages at least 1 hour before testing. Visual cues were placed above each arm of the maze and kept constant during all testing sessions. The test consisted of 2 trials, an acquisition trial and a recognition trial, separated by an inter-trial interval. The first test was performed a week before the end of treatment with a 1-minute inter-trial interval and served to habituate mice to the apparatus. In the acquisition trial of this initial test, the mouse was placed in a pseudo-randomly chosen start arm and allowed to explore the maze freely for 5 minutes with one arm closed (the novel arm). For the inter-trial interval and to control for spontaneous novelty exploration, the mouse was returned to the home cage for 1 minute. In the second (recognition) trial, the mouse was returned to the maze to explore freely with all 3 arms opened for 2 minutes. The actual test was performed a week later using a 2-hour inter-trial interval between the acquisition and recognition trials. The Y-maze was cleaned between trials to eliminate any olfactory cues. The time spent in the novel (previously closed) arm was calculated as the percentage of the total time spent in all arms. The experimenters were blind to the genetic background and treatment and mice were tested in random sequence. The data were analyzed without knowledge of mouse identity.

2.15. Assessing working memory using Y-maze spontaneous alternation paradigm

The working memory test with Y-maze was conducted as described previously (Yau et al., 2007). In this test, all 3 arms of the maze were left open. Mice were placed at the center of the maze with the facing direction randomized for each test. The number and sequence of arm entrances were recorded for 5 minutes. The percent alternation was calculated as the number of alternation (defined as entries into the 3 different arms consecutively) divided by the total possible alternations (the number of arms entered minus 2) multiplied by 100.

2.16. Nesting behavior assessment

Nesting behavior, a type of affiliative behavior, is displayed by both males and females in both parental and nonparental contexts. Mice were individually housed for at least 24 hours in clean plastic cages with approximately 1 cm of corn cob bedding lining the floor and identification cards coded to render the experimenter blind to the sex, age, and genotype of each mouse. Two hours prior to the onset of the dark phase of the lighting cycle, individual cages were

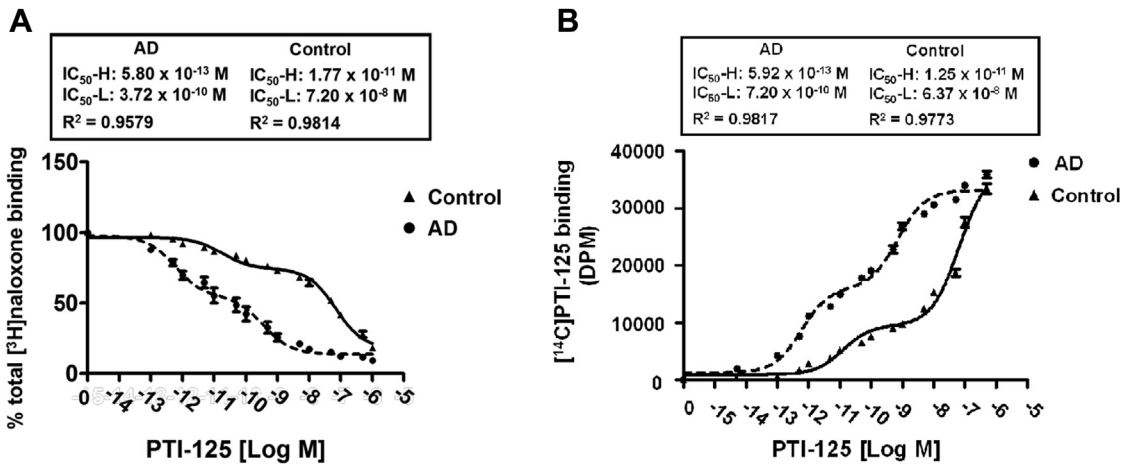

Fig. 1. PTI-125 bound AD postmortem tissue with 580 femtomolar affinity and age-matched control with 18 picomolar affinity, illustrating an altered FLNA conformation and higher binding affinity in diseased brain. A displacement binding assay used a competition curve for the inhibition of [^{3}H]naloxone binding by 16 concentrations of PTI-125 ranging from 0.1 pM to 1 μM in synaptic membranes from postmortem hippocampi of 6 best matched control-AD pairs (A). [C^{14}]PTI-125 (0.05 pM–0.5 μM) binding to FLNA immunopurified from AD and age-matched control tissue confirms that this high-affinity binding is to FLNA, and further illustrates the difference in binding affinity between AD and age-matched control (B). Abbreviations: AD, Alzheimer's disease; FLNA, filamin A.

supplied a 20 cm × 20 cm piece of paper towel cut into approximately 5 cm squared pieces. To reduce variability in housing conditions, mice were tested in counterbalanced groups of mixed genotypes and ages. The next morning (20 hours later) cages were inspected for nest construction. Pictures were taken prior to evaluation for documentation. Paper towel nest construction was scored on a 3-point system (1 = no biting or tears on the paper, 2 = moderate biting and/or tears on the paper but no coherent nest [not grouped into a corner of the cage] and 3 = the vast majority of paper torn into approximately 1 cm pieces and grouped into a corner of the cage). This scoring system was selected after blindly assessing the pictures and noting that the paper towel material was mostly either made into a nest or not disturbed at all (not torn and scattered across the cage). Nestlet nest construction was scored using the established system of Deacon (Wesson and Wilson, 2011).

2.17. Western blot analysis

Solubilized immunoprecipitates derived from coimmunoprecipitation assays were separated by either 7.5 or 10% SDS-PAGE and electrophoretically transferred to nitrocellulose membranes. Membranes were washed with PBS 3 times and blocked overnight at 4 °C with 10% milk in PBS with 0.1% Tween-20 (PBST). Following three 5-minute washes with 0.1% PBST, the membranes were incubated at room temperature for 2 hours with the appropriate antibody at 1:500–1:1000 dilutions. After three 2-minute washes in 0.1% PBST, membranes were incubated for 1 hour with anti-species immunoglobulin G-horseradish peroxidase (1:5000 dilution) and washed with 0.1% PBST 3 times, 2 minutes each. Immunoreactivity was visualized by reacting with chemiluminescent reagent (Pierce ENDOGEN) for exactly 5 minutes and immediate exposure to X-ray film. Specific bands were quantified by densitometric scanning (GS-800 calibrated densitometer, Bio-Rad).

2.18. Statistical analysis

All data are presented as mean ± standard error from the mean. Treatment/group effects were evaluated by one-way analysis of variance followed by Newman–Keul's multiple comparison. Two-tailed Student's *t*-test was also used as the post hoc test for between-group differences. The threshold for significance was $p < 0.05$.

3. Results

3.1. Mechanism of action of PTI-125

PTI-125 was derived from an iterative in silico/in vitro screening process against a known pentapeptide region of FLNA with subsequent medicinal chemistry. Because we previously showed that naloxone and naltrexone bind this site on FLNA (Wang et al., 2008), we were able to show that PTI-125 binds FLNA using a displacement assay. We showed a femtomolar binding affinity for PTI-125 in AD tissue but only picomolar affinity in control brain (Fig. 1A), suggesting an altered conformation of FLNA in AD. Confirmation that FLNA is the high-affinity target of PTI-125 is provided by C^{14}-labeled PTI-125 binding to FLNA immunopurified from AD and age-matched control tissue (Fig. 1B). Impressively, the differential binding affinity between AD and control is maintained after immunopurification of FLNA from these 2 postmortem tissue sources.

To reveal a potential altered conformation of FLNA in AD, we compared the isoelectric focusing point (pI) of FLNA in postmortem AD tissue versus controls. An altered pI reflects a disease-associated conformation (Stucky et al., 2016; Ui, 1973). A shift in pI from 5.9 to 5.3 was detected for FLNA purified from AD tissue, supporting an altered conformation in FLNA in AD brain (Fig. 2A). The pI's were not sensitive to complete dephosphorylation by alkaline phosphatase, indicating that phosphorylation state is not critical to either the native or AD conformation of FLNA. Importantly, PTI-125 incubation at 1 nM for 1 hour largely restored FLNA to its native conformation in each (Fig. 2A). To ascertain whether the conformation reversing effect of PTI-125 is a direct result of FLNA binding, we incubated PTI-125 with a decoy pentapeptide (VAKGL) with the identical sequence of the key PTI-125 binding domain. This pentapeptide is expected to block PTI-125 from binding FLNA and thereby prevents PTI-125's effects. While neither PTI-125 nor the PTI-125/VAKGL combination affected FLNA from control tissues, the pentapeptide blocked PTI-125's ability to restore the AD-related FLNA conformation to FLNA's native form (Fig. 2B). Without the decoy, PTI-125 restored 70.9% ± 3.6% of FLNA to the native conformation; with the decoy, 98.3% ± 0.6% remained in the altered conformation. These data clearly indicate that the reversal of FLNA's altered conformation by PTI-125 requires PTI-125 binding to FLNA.

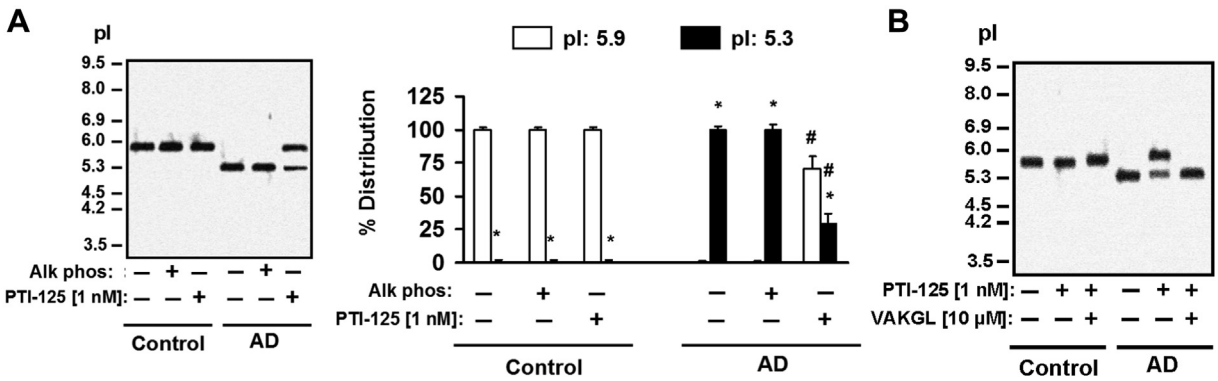

Fig. 2. FLNA conformation is altered in AD. The conformational states of the immunopurified FLNA was analyzed by separating on pH 3–10 isoelectric-focusing gels and then Western blotted with anti-FLNA. (A) FLNA in AD postmortem brain has an isoelectric focusing point (pI) that is shifted from that of FLNA in age-matched control brain. Dephosphorylation by alkaline phosphatase did not alter the conformation, illustrating that the conformations are independent of phosphorylation state. PTI-125 incubation (1 nM) largely restored the conformation of FLNA to its non-AD state. $n = 6$. $^{*}p < 0.00001$ versus non-diseased FLNA conformation (pI 5.9) within group; $^{\#}p < 0.00001$ versus respective FLNA pI in AD without PTI-125 (with or without alk phos). (B) Addition of the decoy pentapeptide VAKGL to prevent PTI-125 binding to FLNA completely blocked PTI-125's ability to restore FLNA's native conformation by PTI-125 (representative isoelectric focusing gel of $n = 4$). Abbreviations: AD, Alzheimer's disease; FLNA, filamin A.

Abnormal FLNA was also found in the ICV $A\beta_{42}$-infused mice from our earlier work (Wang et al., 2012) and in 6- and 10-month 3xTg AD mice with abundant $A\beta_{42}$ and in 10-month wild-type mice with age-dependent $A\beta_{42}$ accumulation. PTI-125 treatment by 2-week intraperitoneal injection in ICV $A\beta_{42}$-infused mice or by 2-month oral administration in 3xTg mice before and after apparent neuropathology and in older wild-type mice restored FLNA to its native conformation (Fig. 3). Importantly, PTI-125 has no effect on the conformation of FLNA in younger wild-type mice with no pathology.

The femtomolar PTI-125 affinity for FLNA in postmortem AD brain or in brains of ICV $A\beta_{42}$-infused mice suggests an extremely low off-rate. To examine this extended retention time, we measured the amount of bound PTI-125 in brains of PTI-125-treated mice in both mouse efficacy studies (Fig. 4). We incubated synaptic membranes from parietal cortices of vehicle- and PTI-125 treated mice with C^{14}-labeled PTI-125 after first washing off any unbound PTI-125. As expected, the vehicle-treated mice in all groups bound the most labeled PTI-125 because there was no PTI-125 from prior treatment to occupy binding sites on FLNA. Of the PTI-125 treated mice, the most C^{14}-PTI-125 binding was seen in the 6-month wild-type mice that showed no pathology, followed by the 10-month wild-type mice with intermediate pathology, followed by the transgenic and ICV $A\beta_{42}$-infused mice. Hence, the ICV $A\beta_{42}$-infused and 3xTg AD mice—with the most FLNA in its diseased conformation—retained the most PTI-125 and the 4-month mice without pathology—and FLNA in its native conformation—retained the least. Because synaptic membranes represent 1% of total tissue, the pg/mg synaptic membranes can be converted to pg/0.1 g of total tissue or pg/0.1 mL for purposes of molarity conversion. The retained PTI-125 bound to FLNA (its only high-affinity target that we know) in tissue is therefore 3 nM for ICV $A\beta_{42}$-infused and 10-month transgenic mice, 2.8 nM for 6-month transgenic mice, 1.9 nM for 10-month wild-type mice, and 0.45 nM for 6-month wild-type mice. These data summarized in Figs. 2–4 confirm that $A\beta_{42}$ induces an altered conformation of FLNA that PTI-125 binds with substantially higher affinity. This femtomolar binding of PTI-125 to the altered conformation survives washing to exert its long-lasting therapeutic benefits, in contrast to the lower-affinity binding of PTI-125 to FLNA in its nondiseased state. These data also confirm that the low nanomolar brain tissue levels are in the range of expected efficacious concentrations based on adult rat

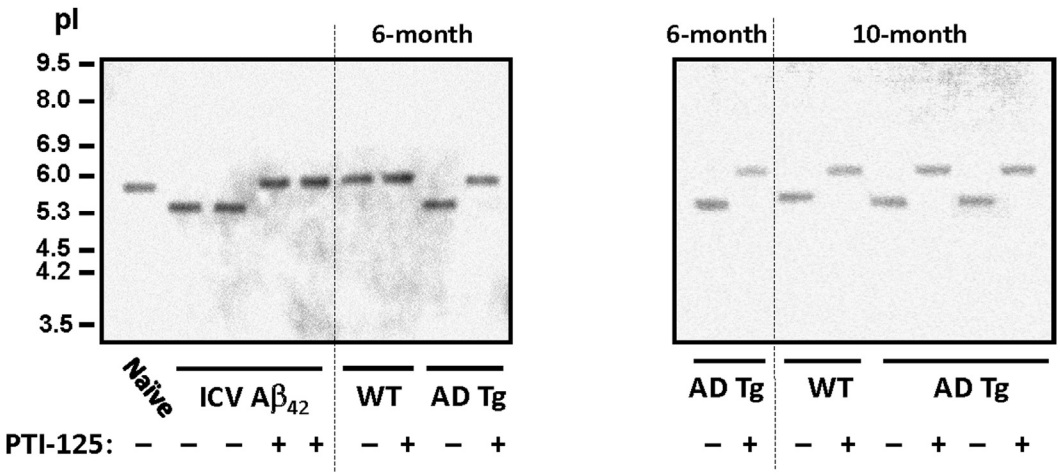

Fig. 3. As in AD postmortem tissue, the pI of FLNA in ICV $A\beta_{42}$-infused, 3xTg AD or aged mice was shifted from 5.9 to 5.3, indicating an altered FLNA conformation induced by $A\beta_{42}$ infusion, by AD or simply age. PTI-125 administration in both in vivo experiments (20 mg/kg intraperitoneal in the ICV $A\beta_{42}$-infused mice and 22 mg/kg oral for transgenic and aged mice) restored this pI to that of the younger or naïve mice. Abbreviations: AD, Alzheimer's disease; FLNA, filamin A; ICV, intra-cerebroventricular; pI, focusing point; 3xTg, triple-transgenic.

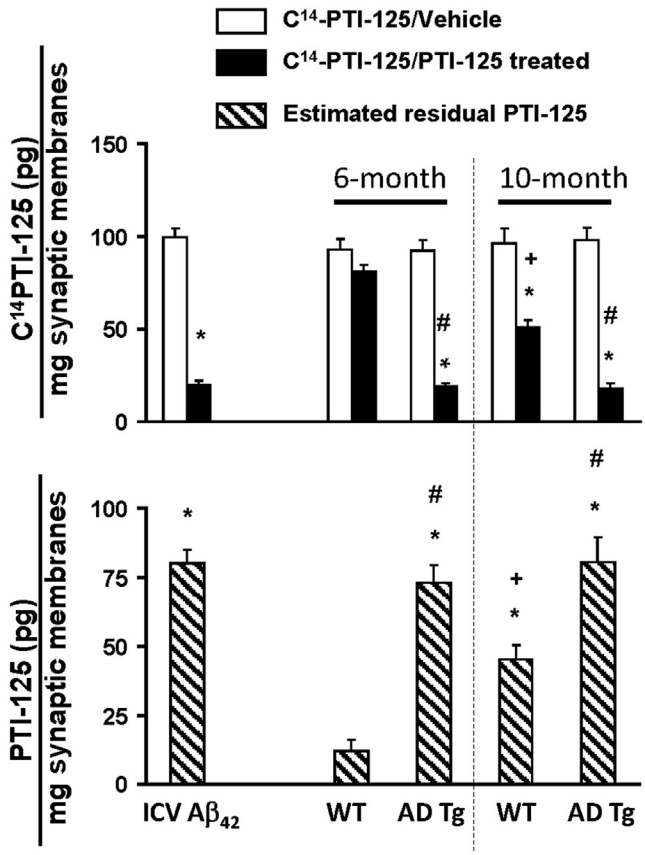

Fig. 4. C^{14}-PTI-125 binding to brains of PTI-125-treated mice illustrated the residual, tightly-bound PTI-125 in both experiments as well as the level of abnormal FLNA with an altered conformation in each. Washed synaptic membranes were incubated with [C^{14}]PTI-125 to assess the levels of PTI-125 binding and residual PTI-125 in the brains of treated animals. Amounts of residual PTI-125 in brains correlated with severity of $A\beta_{42}$ burden with the highest in $A\beta_{42}$-infused mice and transgenic mice, intermediate in aged mice, and least in younger control mice. $^{*}p < 0.01$ versus vehicle in each group; $^{\#}p < 0.01$ versus wildtype in respective age group; $^{+}p < 0.01$ versus 4-month wildtype. Abbreviation: FLNA, filamin A.

brain slice cultures and the current postmortem human tissue experiments.

3.2. In vivo efficacy in 3xTg AD and aged wild-type mice

To establish safety and efficacy of more chronic dosing, we performed a 2-month oral-dosing study in 4-month and 8-month 3xTg AD mice, which show age-dependent progressive neuropathology and associated cognitive deficits. Controls were wild-type 4- and 8-month-old E129 mice that by 10 months showed a notable but milder $A\beta_{42}$ burden and associated pathological effects. PTI-125 via drinking water (22 mg/kg/d) robustly reduced FLNA–α7nAChR/TLR4 associations (Fig. 5A). The reduced FLNA associations in turn resulted in attenuated tau phosphorylation, $A\beta_{42}$–α7nAChR complexes and inflammatory cytokine levels in 3xTg and aged wild-type mice (Fig. 5B–D). This reduction of FLNA–α7nAChR association in hippocampus was mirrored in peripheral blood lymphocytes (data not shown), adding support to our companion biomarker PTI-125-DX. Oral administration of PTI-125 markedly reduced Aβ deposits (Fig. 6) and phosphorylated tau-rich NFTs (Fig. 7) in FCX and hippocampus of 3xTg and 8-month wild-type mice.

The therapeutic benefits of PTI-125 improved function of NMDA and insulin receptors (Fig. 8). NMDAR signaling was assessed by the amounts of NMDA/glycine-induced associated activated key regulatory kinases, Src (pY^{416}Src) and PyK2 (pY^{402}-PyK2) as well as recruited signaling molecules, phospholipase C-γ1 and nNOS and scaffold protein, PSD-95 relative to the obligatory NMDAR subunit NR1 (Fig. 6A). Similarly, 2-month oral administration of PTI-125 also normalized insulin receptor function as indicated by the higher insulin-induced tyrosine-phosphorylated IRβ ($pY^{1150/1151}$ and pY^{960}) and IRS-1 recruitment (Fig. 6B). Importantly, the improved receptor function following 2-month PTI-125 treatment leads to a healthier synaptic activation. This is indicated by a more robust stimulation (by NMDA + glycine) driven expression of the master synaptic plasticity regulator Arc (activity-dependent cytoskeleton-associated protein) in 3xTg and 10-month-old mice (Fig. 6C). These data together indicate that by improving NMDAR and IR function, PTI-125 augments synaptic plasticity.

Although group sizes in this experiment were small for behavioral assessments ($n = 5$ or 6), PTI-125-elicited improvements were noted in nesting behavior (a test of social function) and in spatial and working memory (Fig. 9). PTI-125 significantly improved nesting behavior in 6-month 3xTg AD mice ($p < 0.01$) but the improvement in 10-month 3xTg AD mice was weaker and not significant. On a test of spatial memory, 6-month 3xTg AD mice were significantly impaired compared to 6-month wildtypes ($p < 0.05$), but there was no significant difference between PTI-125–treated 6-month AD transgenics and 6-month wildtypes (treated or untreated). Spatial memory was also impaired in 10-month AD transgenics compared to 6-month wildtypes ($p < 0.01$), and PTI-125 treatment of 10-month 3xTg AD mice significantly improved spatial memory ($p < 0.05$). PTI-125 also significantly improved working memory in 6-month AD transgenic mice ($p < 0.05$).

There were no drug-related findings in histopathology in 6 major organs of these treated mice, supporting PTI-125's safety. Drug exposure from this 2-month study was 1532 ± 86.7 ng/mL (5.9 μM) in plasma and 4.94 ± 1.17 ng/g (19 nM) in brain homogenate (of wildtype mice), easily in excess of the effective dose range of 1 pM to 1 nM in ex vivo postmortem human brain slices. These exposure data were obtained with an LC-MS/MS bioanalytical method for plasma that has since been validated for good laboratory practice use.

3.3. Ex vivo efficacy in postmortem AD hippocampus

PTI-125's restoration of receptor function, improved synaptic plasticity and reduced tau hyperphosphorylation that were seen in vivo were also demonstrated in our ex vivo experiments with postmortem human brain tissue. We demonstrated that 1 hour incubation of 1 nM PTI-125 is effective in normalizing receptor activities in AD frontal cortices (Wang et al., 2012). To address the dose-dependency of PTI-125 effects, we further investigated the efficacy of lower concentrations that are closer to PTI-125's femtomolar binding affinity in the current ex vivo experiments. Postmortem hippocampal slices from 5 pairs of AD patients and age-matched controls were incubated for 1 hour with a concentration range of 1 pM–1 nM PTI-125. We also examined hippocampus to demonstrate that the effects of PTI-125 are not unique to the region earlier tested (FCX). In this study, subnanomolar concentrations of PTI-125 elicited the same beneficial effects previously shown with 1 nM PTI-125, although the magnitude of those effects were lower at 10 and 1 pM than at 100 pM or 1 nM, demonstrating a clear dose-response. We also noted that the impairments in hippocampus were more severe than those noted earlier in FCX from the same (plus 6 additional) patients (Wang et al., 2012).

PTI-125 dose-dependently reduced $A\beta_{42}$-induced FLNA coupling to α7nAChR and TLR4 in both $A\beta_{42}$-treated control and AD hippocampus (Fig. 10A). FLNA–TLR4 coupling was reduced starting at 10 pM in AD tissue and at 1 pM in $A\beta_{42}$-treated control.

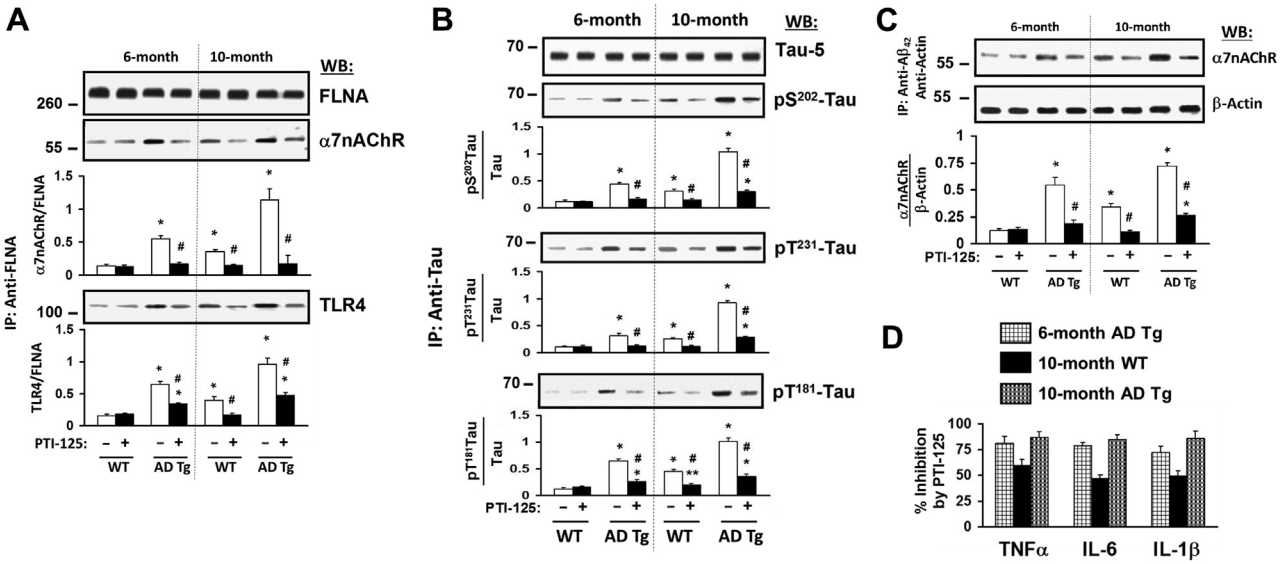

Fig. 5. Two-month administration of PTI-125 via drinking water (~22 mg/kg/d) to wild-type or 3xTg AD mice starting at 4 or 8 months of age reduced tau phosphorylation (A) and $A\beta_{42}$-α7nAChR complexes (B) in frontal cortex of 3xTg AD or the older wild-type mice. Demonstrating its mechanism of action, PTI-125 also reduced FLNA association with α7nAChR and TLR4 (C). Synaptosomes prepared from frontal cortex were immunoprecipitated with anti-tau or anti-$A\beta_{42}$ antibodies, and levels of phosphorylated tau (at 3 phosphoepitopes) or α7nAChR were respectively detected by Western blots (WB; insets) and quantified by densitometric quantitation. PTI-125 also reduced inflammatory cytokine levels in 8-month mice, measured by a fluorescence ELISA assay (D). $n = 6$. $^{*}p < 0.01$ and $^{**}p < 0.05$ versus 4-month mice; $^{\#}p < 0.01$ versus vehicle-treated 8-month mice. Abbreviations: α7nAChR, α7-nicotinic acetylcholine receptor; FLNA, filamin A; TLR4, toll-like receptor 4; 3xTg, triple-transgenic.

A concentration of 1 pM was sufficient to produce a significant reduction in FLNA–α7nAChR interaction in both tissues. As a consequence, PTI-125 incubation dose-dependently reduced $A\beta_{42}$–α7nAChR complexes in postmortem AD or $A\beta_{42}$-treated age-matched control hippocampus starting at 1 pM (Fig. 10B). In $A\beta_{42}$-treated control hippocampus, PTI-125 dose-dependently

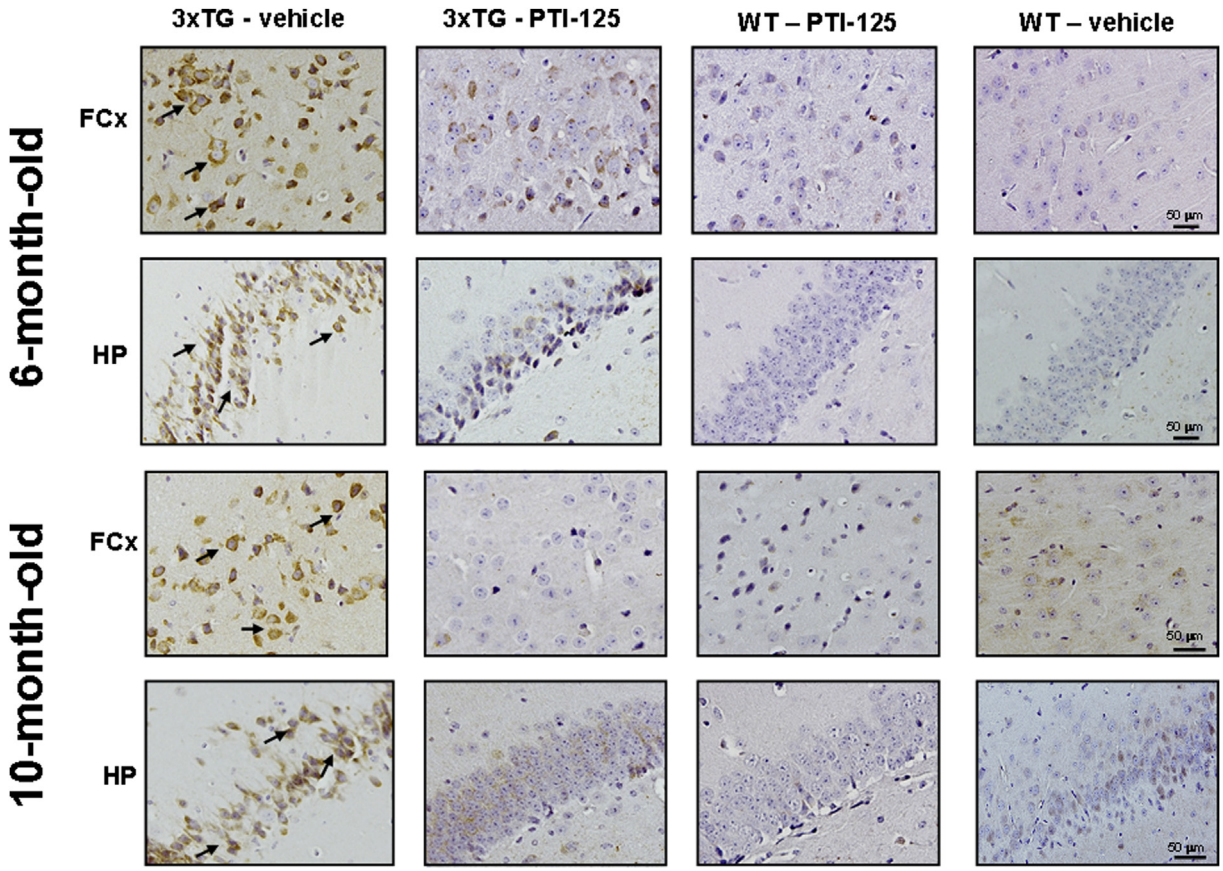

Fig. 6. Representative sections immunostained with anti-$A\beta_{42}$ antibodies show that PTI-125 treatment reduced $A\beta_{42}$ deposits in hippocampus and frontal cortex of both transgenic and older wild-type mice. Arrows indicate examples of $A\beta_{42}$ aggregates.

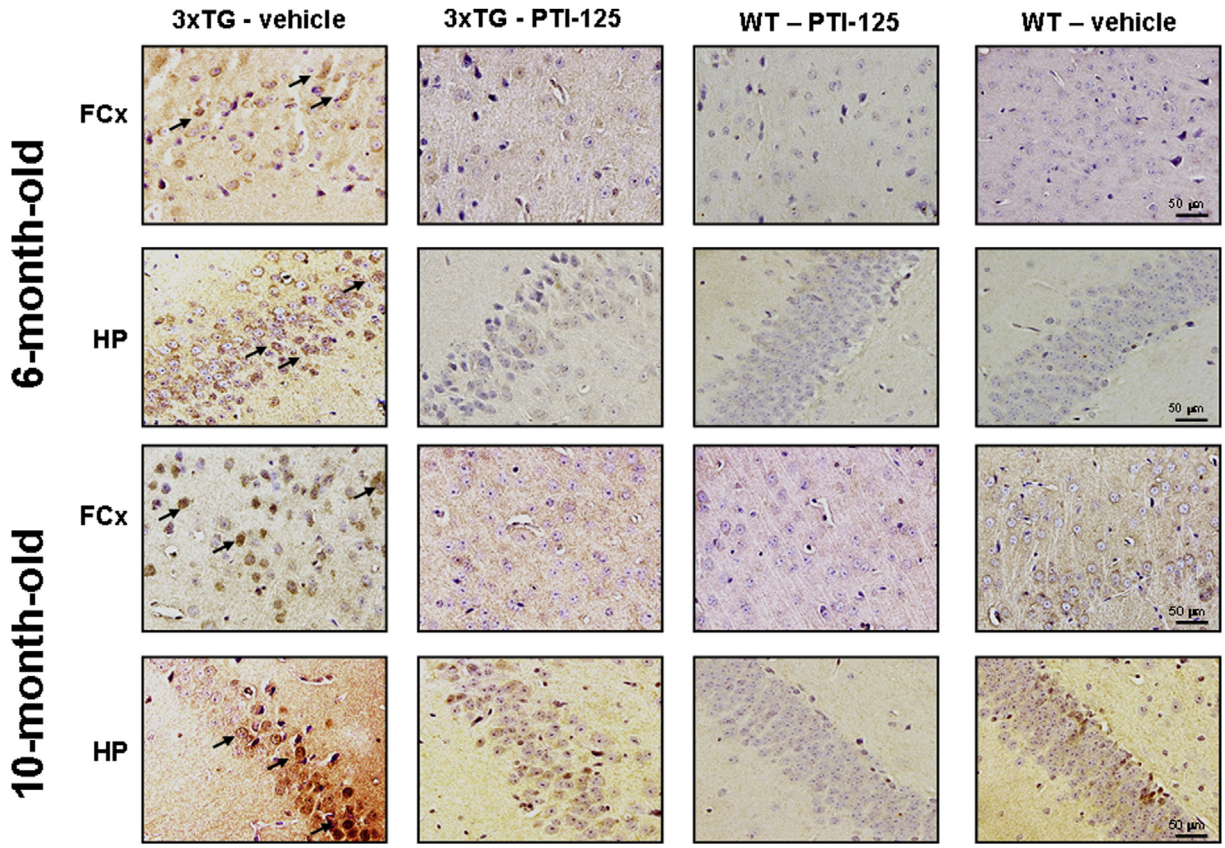

Fig. 7. Representative sections immunostained with anti-NFT (phospho-tau) antibodies show that PTI-125 treatment reduced NFT immunoreactivity in hippocampus and frontal cortex of both transgenic and older wild-type mice. Arrows indicate examples of hyperphosphorylated tau-rich NFTs. Abbreviation: NFT, neurofibrillary tangle.

reduced phosphorylated tau as well as tau nitration, an indicator of oxidative stress started at 1 pM (Fig. 11).

Similarly, PTI-125 dose-dependently restored NMDA receptor signaling that is impaired in postmortem AD or $A\beta_{42}$-treated age-matched control hippocampus (Fig. 12). Both $A\beta_{42}$-treated control hippocampus and AD hippocampus showed approximately 70% reduction in NMDAR activity evidenced as reduced NMDA/glycine-induced Src and Pyk2 activation and recruitment of

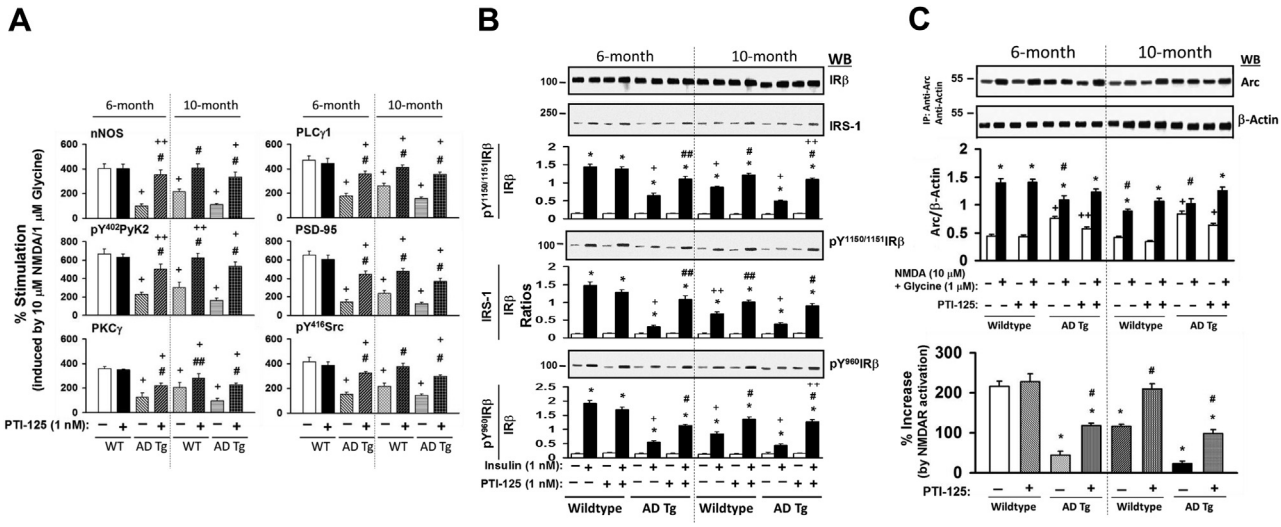

Fig. 8. PTI-125 via drinking water reduced the impairment in NMDAR (A) and IR (B) signaling. The coimmunoprecipitation assay for NMDAR signaling measured by the levels of NMDA/glycine-induced association of activated kinases and signaling molecules with NMDARs as the ratios of 6 different NMDAR-linked signaling molecules to NR1, the obligatory subunit of NMDAR. IR function was measured by the tyrosine phosphorylation of IRβ and the level of the signaling adapter molecule IRS-1 recruited. NMDA/glycine-induced expression of the synaptic plasticity master regulator Arc was also impaired in 3xTg AD and aged mice (C). Total Arc was immunoprecipitated along with actin (immunoprecipitation and loading control) and analyzed by Western blotting. These impairments were ameliorated by PTI-125 oral administration (A, B, and C). Blots (inset) were analyzed by densitometric quantitation. $n = 6$. $^{*}p < 0.01$ versus unstimulated control; $^{\#}p < 0.01$ and $^{\#\#}p < 0.05$ versus vehicle; $^{+}p < 0.01$ and $^{++}p < 0.05$ versus 4-month mice. Abbreviations: AD, Alzheimer's disease; IRS-1, Insulin receptor substrate 1; NR1, NMDA receptor subunit 1; 3xTg, triple-transgenic.

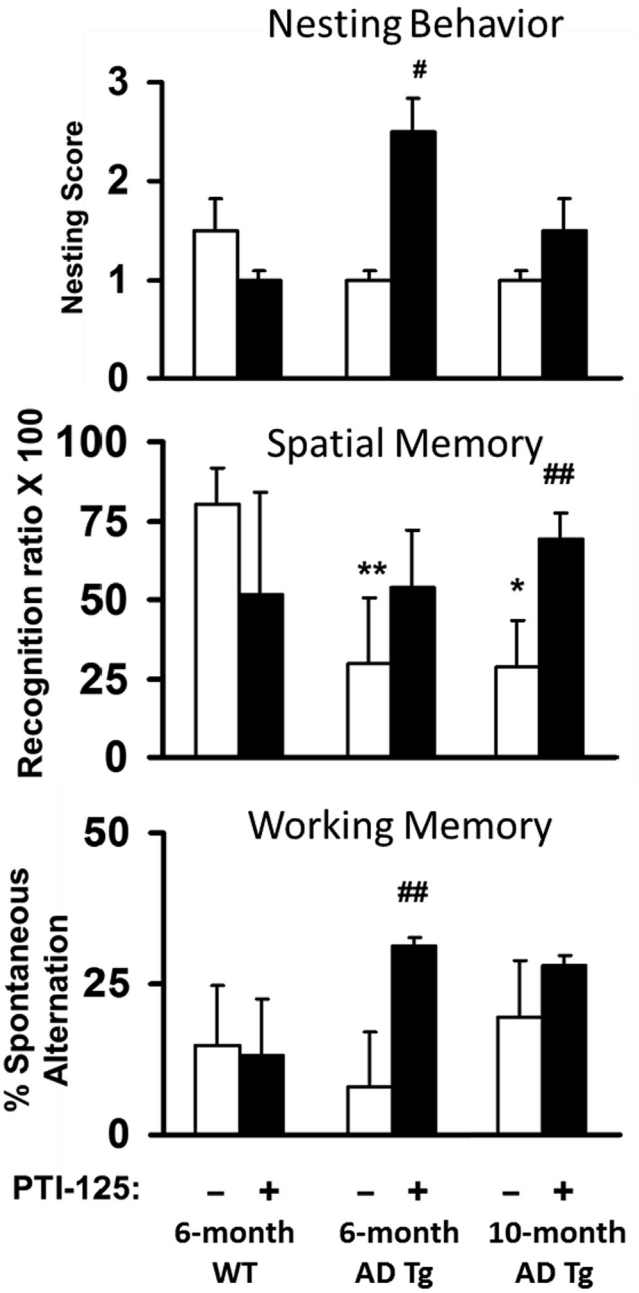

Fig. 9. PTI-125 via drinking water improved nesting behavior in 6-month 3xTg AD mice. Compared to 6-month wildtypes, spatial memory assessed using Y-maze with extra-maze visual cues was impaired in 3xTg AD mice of both ages but not in 3xTg AD mice of either age treated with PTI-125. Additionally, PTI-125 significantly improved spatial memory in 10-month 3xTg AD mice. PTI-125 significantly improved working memory assessed by Y-maze spontaneous alternation paradigm in the 10-month but not 6-month 3xTg AD mice. $n = 5$. $^{*}p < 0.01$, $^{**}p < 0.05$ versus 6-month-old vehicle-treated wild-type group; $^{\#}p < 0.01$, $^{\#\#}p < 0.05$ versus respective vehicle-treated group. Abbreviations: AD, Alzheimer's disease; 3xTg, triple-transgenic.

phospholipase C-γ1, nNOS and PKCγ compared to age-matched controls. In concert, these 6 indices of NMDAR dysfunction were dose-dependently ameliorated by PTI-125 (Fig. 12).

The improved NMDAR function by ex vivo PTI-125 incubation correlates with the efficacy in restoring NMDAR-activation induced Arc expression, indicating restored synaptic plasticity even at 1 pM (Fig. 13). In summary, PTI-125 produced significant beneficial effects starting at 1 pM in $A\beta_{42}$-treated control hippocampus on all parameters and at 1 or 10 pM in AD postmortem hippocampus in assays appropriate for AD postmortem tissue (these exclude tau phosphorylation and Arc expression). These results illustrate a PTI-125 dose-response from 1 pM to 1 nM concentrations, with maximal effects at 100 pM or 1 nM, corroborating our earlier unpublished data in adult rat brain slice cultures that showed peak effects on NMDAR and α7nAChR function at 1 nM with 10 nM a saturating concentration.

4. Discussion

Our early work identified the critical role of FLNA in $A\beta_{42}$ signaling via α7nAChR and TLR4 that leads to tau hyperphosphorylation and neuroinflammation (Wang et al., 2012). We now show that $A\beta_{42}$ can induce an altered conformation of this ubiquitous scaffolding protein to intensify AD pathogenesis. By reversing FLNA to its native, nondiseased state, PTI-125 attenuates $A\beta_{42}$-driven toxic events that ultimately result in tau hyperphosphorylation, receptor dysfunctions, impaired synaptic plasticity, and oxidative stress leading to neurofibrillary lesions, NFTs, and $A\beta_{42}$ deposits as well as neurodegeneration. PTI-125's preferential binding to the altered FLNA conformation is indicated by a femtomolar affinity for FLNA in synaptic membranes or immunopurified from postmortem human AD hippocampus, compared to a picomolar affinity for FLNA in age-matched control hippocampus. Importantly, PTI-125's lower-affinity binding to native FLNA does not further change its conformation or have any apparent effects. This differential binding affinity renders the binding site markedly more accessible in the disease state and explains PTI-125's efficacy at low doses and low toxicities despite a ubiquitous target. The unique ability for PTI-125 to bind and restore pathological FLNA to its native conformation suggests that PTI-125 is a disease-modifying therapeutic agent for diseases with abnormally heightened amyloid pathologies such as AD. Once FLNA is reversed to its native conformation, the affinity of PTI-125 becomes considerably lower, leading to its release.

The multiple beneficial effects of PTI-125 were initially demonstrated in an acute (2-week) ICV $A\beta_{42}$ infusion mouse model and in postmortem human AD brain incubated with 1 nM PTI-125 for 1 hour. The present work extends these findings to a more chronic and oral administration in 3xTg AD mice, with treatment starting either at 4 months, when neuropathology such as Aβ deposits is not yet apparent or at 8 months, when the neuropathology is established in these mice. The 8-month wildtypes, a control for the 8-month 3xTg AD mice, showed age-dependent Aβ burden and associated neuropathologies by 10 months that were milder than in transgenics of either age. In 3xTg AD and older wild-type mice, PTI-125 administration for 2 months via drinking water improved receptor activities (indicated by restored receptor signaling) and synaptic plasticity (indicated by normalized NMDAR activation-mediated expression of the master synaptic plasticity regulator Arc). These functional benefits were associated with improvements in nesting behavior and spatial and working memory in transgenic mice, even in small group sizes. The molecular functional results closely replicate our earlier published findings in the ICV $A\beta_{42}$-infused mice treated with 2-week PTI-125 injections as well as in postmortem human AD brain (1-h ex vivo PTI-125 incubation). By decreasing the levels of FLNA–α7nAChR and TLR4 associations, PTI-125 markedly reduces $A\beta_{42}$-induced tau phosphorylation and inflammatory cytokine levels to a near nondisease state. These therapeutic effects are supported by the marked reduction in $A\beta_{42}$ deposits and phosphorylated tau-containing NFTs. Additionally, the AD pathologies noted in normal, aged mice prior to cognitive impairment supports the hypotheses that aging is a contributing factor of AD pathogenesis and that AD pathologies are initiated at least a decade ahead of apparent cognitive decline in humans. The

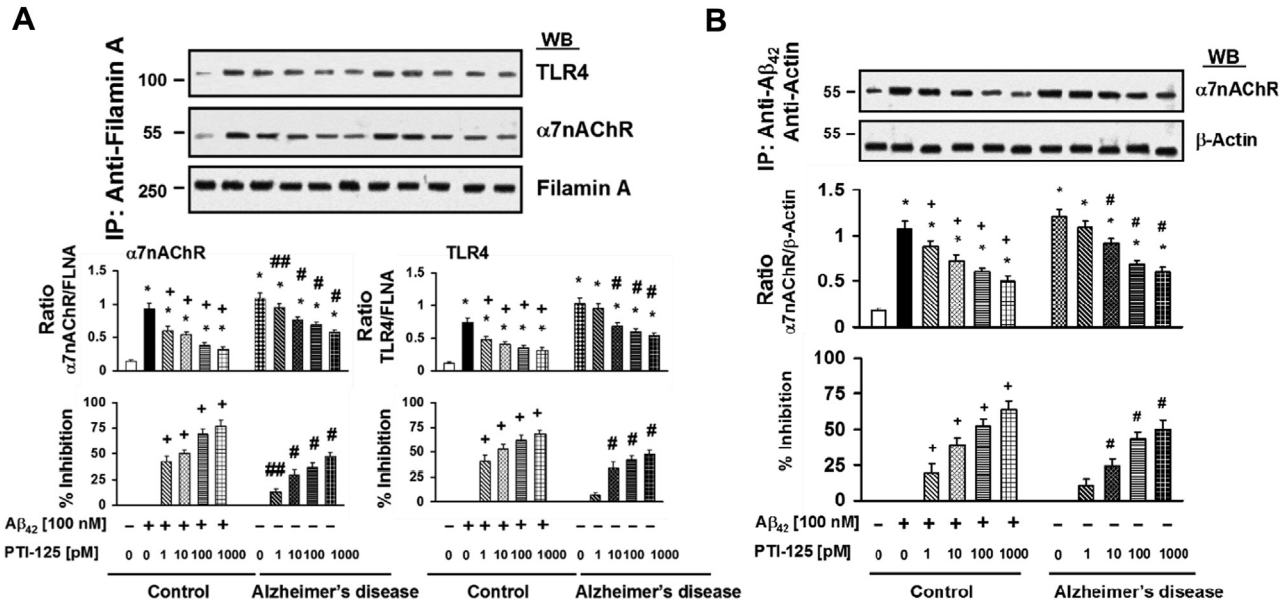

Fig. 10. PTI-125 (1 hour) dose-dependently reduced FLNA association with α7nAChR and with TLR4 in postmortem AD and $A\beta_{42}$-treated age-matched control hippocampal slices (A). PTI-125 similarly dose-dependently reduced $A\beta_{42}$-α7nAChR complexes with statistical significance starting at 1 pM in $A\beta_{42}$-treated age-matched control and at 10 pM in AD hippocampus (B). Synaptosomes prepared from postmortem hippocampus from 5 best-matched control/AD pairs were incubated with vehicle, PTI-125 or PTI-125 + $A\beta_{42}$ (control), solubilized and immunoprecipitated with immobilized anti-FLNA, and α7nAChR, and TLR4 levels in the immunoprecipitates were detected by Western blot using specific antibodies. Blots (inset) were analyzed by densitometric quantitation. $n = 5$. $^{*}p < 0.01$ versus vehicle-treated age-matched control; $^{+}p < 0.01$ versus $A\beta_{42}$-treated age-matched control; $^{\#}p < 0.01$ and $^{\#\#}p < 0.05$ versus vehicle-treated AD. Abbreviations: α7nAChR, α7-nicotinic acetylcholine receptor; AD, Alzheimer's disease; FLNA, filamin A; TLR4, toll-like receptor 4.

multiple effects of PTI-125 indicate improved neuronal heath and reduced pathophysiology in both AD and normal aging.

We also investigated a concentration range for PTI-125 in postmortem hippocampus, extending our earlier findings in frontal cortical slices that used a single 1 nM concentration. Using concentrations that are closer to PTI-125's femtomolar affinity for FLNA, we now demonstrate that 1-hour incubation with concentrations as low as 1 pM dose-dependently reduce neuropathologies detected in postmortem human AD hippocampus or in $A\beta_{42}$-treated age-matched control hippocampus. These PTI-125 effects include improved NMDAR function, reduced tau hyperphosphorylation, reduced $A\beta_{42}$–α7nAChR complexes, and reduced FLNA association with α7nAChR or TLR4. PTI-125 also reduced tau nitration, a marker of oxidative stress, and improved synaptic plasticity as indicated by the activity-driven expression of the master synaptic regulator, Arc. Together with the preferential binding and reversal of the pathologic FLNA conformation, these ex vivo data show that PTI-125 is potent and highly efficacious in normalizing receptor function and reducing Aβ-driven pathologies.

Though other targets have been demonstrated for soluble $A\beta_{42}$, $A\beta_{42}$ generally binds these targets with high nanomolar or lower affinities, suggesting high off-rates and limited target engagement. In contrast, $A\beta_{42}$'s subpicomolar affinity for α7nAChR suggests it is nearly irreversible, offering one explanation for the many clinical trial failures of anti-Aβ antibodies. With its unique mechanism of action, PTI-125 noncompetitively reduces $A\beta_{42}$'s affinity for α7nAChR by 1000- to 10,000-fold (Wang et al., 2012). $A\beta_{42}$'s greatly reduced binding affinity prevents its toxic signaling, reduces $A\beta_{42}$ accumulation on α7nAChRs and even dissociates bound $A\beta_{42}$ from α7nAChR in postmortem AD brain as shown here and previously (Wang et al., 2012). Interestingly, the femtomolar binding of PTI-125 to altered FLNA has a long retention time in brain to exert its beneficial effects, evidenced by [C^{14}]PTI-125 binding in brains of treated and untreated ICV $A\beta_{42}$-infused or aged mice. This tight binding was indicated by residual PTI-125 that survived washing of brain tissue. The higher levels of residual bound PTI-125 in ICV $A\beta_{42}$-infused or 3xTg AD versus naïve wild-type mice and in older versus younger mice is further evidence that PTI-125's high-affinity binding is to the diseased/age-related conformation of FLNA.

Other targets of soluble Aβ include PrP^{C}, a prion receptor, which Aβ binds with 50–100 nanomolar affinity to suppress long-term potentiation in slice cultures (Lauren et al., 2009). Acting as a coreceptor for the Aβ–PrP^{C} complex, mGluR5 also plays a role in the impaired long-term potentiation (Um et al., 2013). Importantly, PTI-125 significantly restored synaptic plasticity as illustrated by increasing activity-driven expression of the master regulator Arc. Soluble Aβ has also been shown to bind neuroligin-1, a membrane-bound postsynaptic cell adhesion protein important to postsynaptic receptor clustering and synaptic integrity. Aβ's nanomolar binding to neuroligin-1 is proposed to promote Aβ oligomer formation (Dinamarca et al., 2011). It should be noted that soluble Aβ in monomeric or oligomeric form can signal through α7nAChR (Tong et al., 2011; Wang et al., 2000a,b, 2003). Further, amyloid-induced microglial activation and neuroinflammation were shown to suppress neuroligin-1 expression through an epigenetic modification of neuroligin-1 promoter. Manipulating the inflammation modulated the promoter, glutamatergic transmission in the hippocampus and memory (Bie et al., 2014). Though untested, PTI-125 should also restore neuroligin-1 expression due to PTI-125's profound reduction of neuroinflammation.

Despite the lower-affinity of Aβ binding to other targets, it is difficult to assess the relative contributions of these other Aβ targets or other potential disease mechanisms to overall AD neuropathology. However, the hyperphosphorylation of tau, effected by $A\beta_{42}$'s signaling via α7nAChR to activate ERK1 and JNK, disrupts tau's normal function of assembling and stabilizing microtubules, critical to general neuronal processes (Stoothoff and Johnson, 2005). Dysfunctional tau and dysfunctional microtubules could impede axonal transport, leading to a wide variety of impaired neuronal function (Buee et al., 2000; Stoothoff and Johnson, 2005;

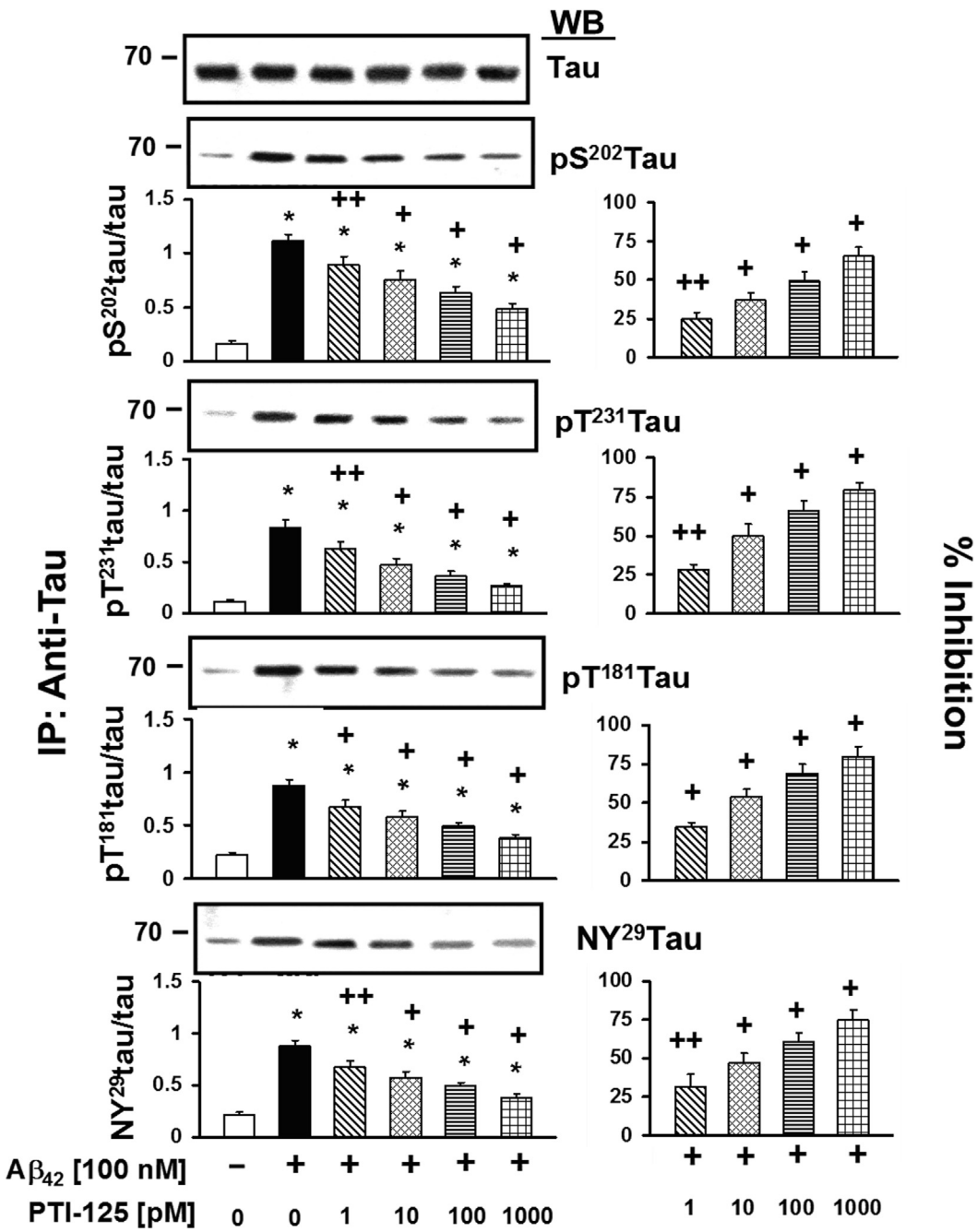

Fig. 11. PTI-125 dose-dependently decreased $A\beta_{42}$-induced tau phosphorylation at Ser-202, Thr-231, and Thr-181 in control human hippocampus. Levels of tau protein phosphorylated at each site were measured in the immunoprecipitates of a pan anti-tau antibody that did not distinguish its phosphorylation state by Western blotting with specific antibodies separately recognizing each tau phosphoepitope. Blots (inset) were analyzed by densitometric quantitation. $n = 5$. $^{*}p < 0.01$ versus vehicle/vehicle; $^{+}p < 0.01$ and $^{++}p < 0.05$ versus $A\beta_{42}$/vehicle.

Wang et al., 2013). The beneficial impact of PTI-125 on a range of AD-related neuropathologies, achieved by blocking $A\beta_{42}$'s signaling to hyperphosphorylate tau, supports this theory. Neuroinflammation is an additional, prominent AD neuropathology that likely also impedes neuronal function. Suppressing both $A\beta_{42}$-induced toxic signaling via α7nAChRs and TLR4 signaling by binding a single target strengthens the potential broad-spectrum therapeutic impact of PTI-125.

In summary, $A\beta_{42}$'s femtomolar binding affinity to α7nAChR, its aberrant signaling and the required FLNA–α7nAChR association can all be markedly attenuated by restoring FLNA to its native conformation. The result is a prevention of $A\beta_{42}$ accumulation and the toxic signaling that hyperphosphorylates tau, drives plaque and neurofibrillary pathologies, and ultimately, neurodegeneration. Most importantly, PTI-125 alleviates deficits in synaptic plasticity, including those modulated by NMDARs. PTI-125's additional abilities to reduce insulin resistance, another prominent AD pathology, to markedly reduce neuroinflammation by attenuating TLR4 signaling, and to minimize oxidative stress as evidenced by reducing $A\beta_{42}$-induced tau nitration should also benefit synaptic transmission and improve neuronal resilience. The myriad of beneficial effects by this promising novel therapeutic candidate

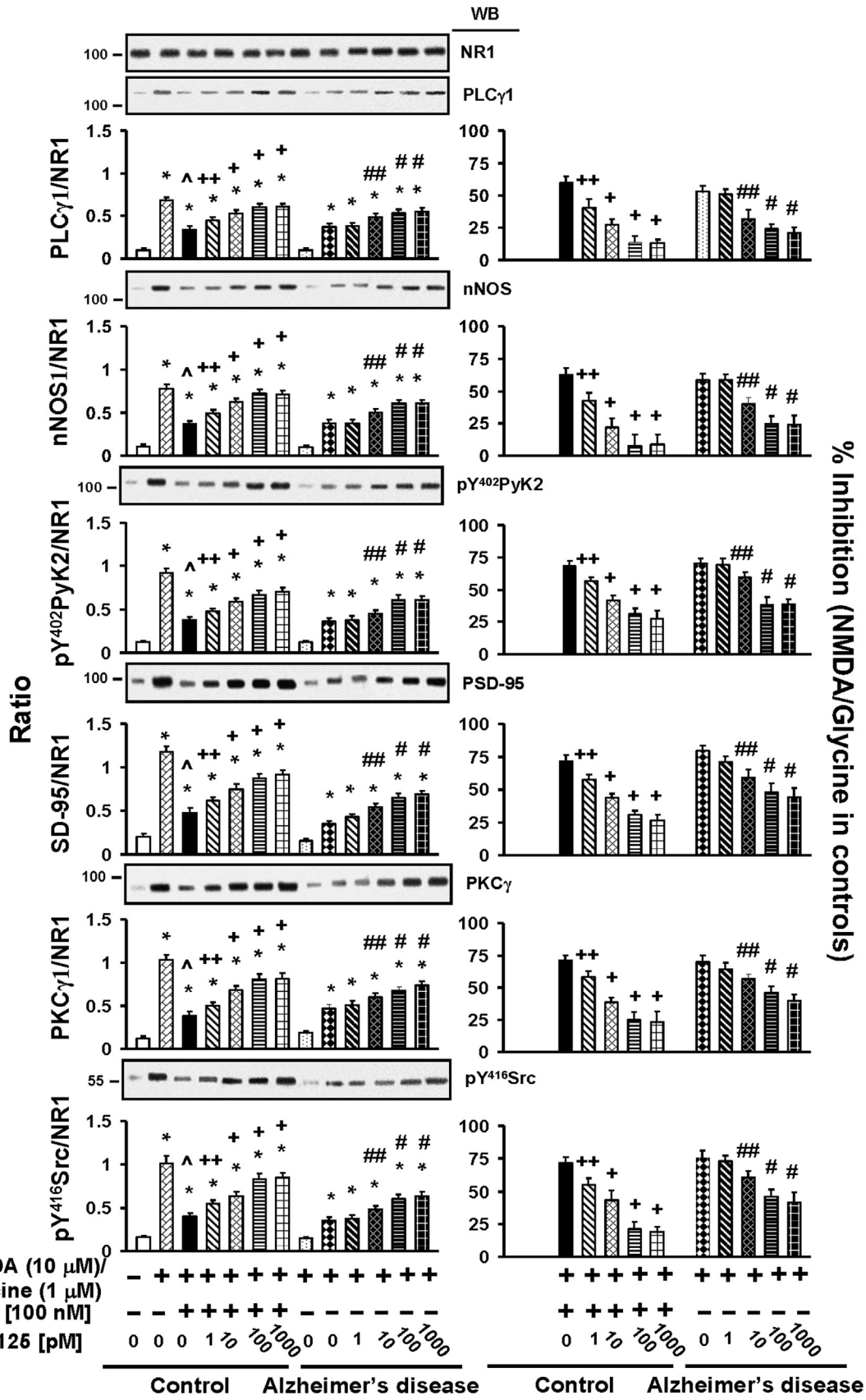

Fig. 12. In postmortem AD and $A\beta_{42}$-treated age-matched control hippocampus, PTI-125 (1 hour) dose-dependently improved NMDAR function, evidenced by the levels of 6 signaling molecules coimmunoprecipitated with NMDARs using antibodies against NR1, the NMDAR obligatory subunit. Blots (inset) were analyzed by densitometric quantitation. $n = 5$. $^{*}p < 0.01$ versus control basal; $^{\wedge}p < 0.01$ $A\beta_{42}$ + NMDA/glycine versus NMDA/glycine; $^{+}p < 0.01$ and $^{++}p < 0.05$ versus $A\beta_{42}$ in controls; $^{\#}p < 0.01$ and $^{\#\#}p < 0.05$ versus AD NMDA/glycine. Abbreviations: AD, Alzheimer's disease; NR1, NMDA receptor subunit 1.

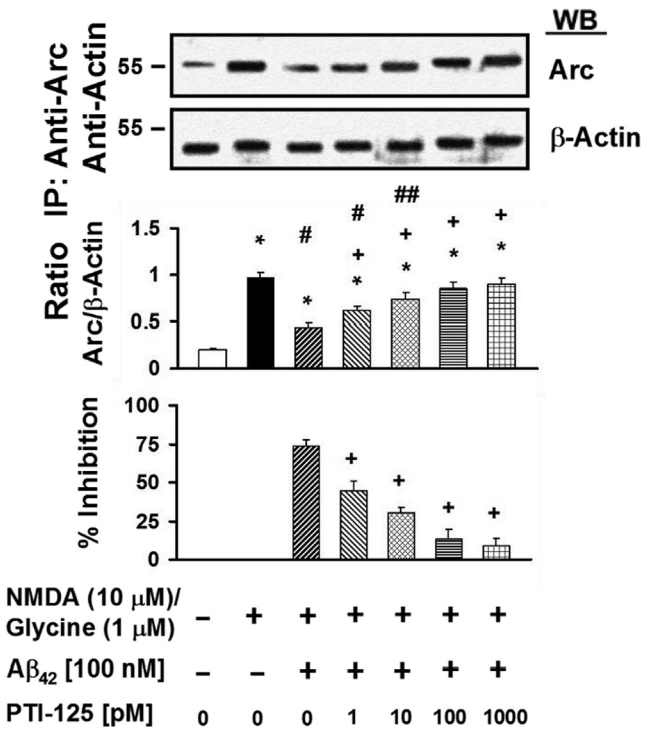

Fig. 13. In control hippocampus, $A\beta_{42}$ impaired NMDA/glycine-induced expression of the master synaptic plasticity regulator, Arc. PTI-125 dose-dependently improved NMDA/glycine-induced Arc expression. Control hippocampal slices were incubated with $A\beta_{42}$ alone or $A\beta_{42}$ + PTI-125 (1 pM–1 nM). Tissues solubilized and Arc was immunoprecipitated along with actin (served as immunoprecipitation/loading control). The levels of Arc and β-actin were determined by Western blotting. Blots (inset) were analyzed by densitometric quantitation. $n = 5$. $^{*}p < 0.01$ versus basal; $^{\#}p < 0.01$ and $^{\#\#}p < 0.05$ versus NMDA/glycine control; $^{+}p < 0.01$ versus $A\beta_{42}$ + NMDA/glycine.

validates FLNA as an important novel target and reinforces $A\beta_{42}$ signaling via α7nAChR and TLR4 as prominent pathogenic mechanisms in AD. PTI-125's mechanism of action, reversing proteopathy by binding and restoring the disease-altered protein conformation to its nondiseased state, underscores the importance of protein conformation in neuronal health and disease.

Disclosure statement

PTI-125 is a proprietary compound of Pain Therapeutics, Inc (PTI). Dr. Burns is an employee and Dr. Wang is a consultant for this company.

Acknowledgements

PTI funded this work except for the C^{14}-labeling of PTI-125, which was produced for biodistribution studies under NIH grant number 4R44AG050301. The authors thank Dr. Frank LaFerla for the transgenic mice provided to HYW under Material Transfer Agreement. The authors also thank Dr. Kaliris Salas-Ramirez, Marissa Goberdhan, MS, and Sanket M. Shah, MS, for helping with behavioral tests.

References

Bateman, R., Xiong, C., Benzinger, T., Fagan, A., Goate, A., Fox, N., Marcus, D.S., Cairns, N.J., Xie, X., Blazey, T.M., Holtzman, D.M., Santacruz, A., Buckles, V., Oliver, A., Moulder, K., Aisen, P.S., Ghetti, B., Klunk, W.E., McDade, E., Martins, R.N., Masters, C.L., Mayeux, R., Ringman, J.M., Rossor, M.N., Schofield, P.R., Sperling, R.A., Salloway, S., Morris, J.C., Dominantly Inherited Alzheimer Network, 2012. Clinical and biomarker changes in dominantly inherited Alzheimer's disease. NEJM 367, 795–804.

Bie, B., Wu, J., Yang, H., Xu, J., Brown, D., Naguib, M., 2014. Epigenetic suppression of neuroligin 1 underlies amyloid-induced memory deficiency. Nat. Neurosci. 17, 223–231.

Buee, L., Bussiere, T., Buee-Scherrer, V., Delacourte, A., Hof, P., 2000. Tau protein isoforms, phosphorylation and role in neurodegenerative disorders. Brain Res. Rev. 33, 95–130.

D'Andrea, M., Nagele, R., 2006. Targeting the alpha 7 nicotinic acetylcholine receptor to reduce amyloid accumulation in Alzheimer's disease pyramidal neurons. Curr. Pharm. Des. 12, 677–684.

D'Andrea, M., Nagele, R., Wang, H.-Y., Peterson, P., Lee, D., 2001. Evidence that neurones accumulating amyloid can undergo lysis to form amyloid plaques in Alzheimer's disease. Histopathology 38, 120–134.

Dinamarca, M., Weinstein, D., Monasterio, O., Inestrosa, N., 2011. The synaptic protein neuroligin-1 interacts with the amyloid β-peptide. Is there a role in Alzheimer's disease? Biochemistry 50, 8127–8137.

Dineley, K., Bell, K., Bui, D., Sweatt, J., 2002. β-Amyloid peptide activates α7 nicotinic acetylcholine receptors expressed in xenopus oocytes. J. Biol. Chem. 277, 25056–25061.

Dziewczapolski, G., Glogowski, C., Masliah, E., Heinemann, S., 2009. Deletion of the alpha 7 nicotinic acetylcholine receptor gene improves cognitive deficits and synaptic pathology in a mouse model of Alzheimer's disease. J. Neurosci. 29, 8805–8815.

Haass, C., Selkoe, D., 2007. Soluble protein oligomers in neurodegeneration: lessons from the Alzheimer's amyloid beta-peptide. Nat. Rev. Mol. Cell Biol. 8, 101–112.

Hefter, D., Kaiser, M., Weyer, S., Papageorgiou, I., Both, M., Kann, O., Müller, U.C., Draguhn, A., 2016. Amyloid precursor protein protects neuronal network function after hypoxia via control of voltage-gated calcium channels. J. Neurosci. 36, 8356–8371.

Hu, M., Waring, J., Gopalakrishnan, M., Li, J., 2008. Role of GSK-3beta activation and alpha7 nAChRs in Abeta(1-42)-induced tau phosphorylation in PC12 cells. J. Neurochem. 106, 1371–1377.

Hyman, B., Trojanowski, J., 1997. Consensus recommendations for the postmortem diagnosis of Alzheimer disease from the National Institute on Aging and the Reagan Institute Working Group on diagnostic criteria for the neuropathological assessment of Alzheimer disease. J. Neuropathol. Exp. Neurol. 56, 1095–1097.

Inestrosa, N., Godoy, J., Vargas, J., Arrazola, M., Rios, J., Carvajal, F., Serrano, F.G., Farias, G.G., 2013. Nicotine prevents synaptic impairment induced by amyloid-β oligomers through α7-nicotinic acetylcholine receptor activation. Neuromolecular Med. 15, 549–569.

Lauren, J., Gimbel, D., Nygaard, H., Gilbert, J., Strittmatter, S., 2009. Cellular prion protein mediates impairment of synaptic plasticity by amyloid-beta oligomers. Nature 457, 1128–1132.

McKhann, G., Drachman, D., Folstein, M., Katzman, R., Price, D., Stadlan, E., 1984. Clinical diagnosis of Alzheimer's disease: report of the NINCDS-ADRDA Work Group under the auspices of Department of Health and Human Services Task Force on Alzheimer's disease. Neurology 34, 939–944.

Medeiros, R., Castello, N., Cheng, D., Kitazawa, M., Baglietto-Vargas, D., Green, K., Esbenshade, T.A., Bitner, R.S., Decker, M.W., LaFerla, F.M., 2014. α7 Nicotinic receptor agonist enhances cognition in aged 3xTg-AD mice with robust plaques and tangles. Am. J. Pathol. 184, 520–529.

Nagele, R., D'Andrea, M., Anderson, W., Wang, H.-Y., 2002. Accumulation of beta-amyloid1-42 in neurons is facilitated by the alpha7 nicotinic acetylcholine receptor in Alzheimer's disease. Neuroscience 110, 199–211.

Näslund, J., Haroutunian, V., Mohs, R., Davis, K., Davies, P., Greengard, P., Buxbaum, J.D., 2000. Correlation between elevated levels of amyloid betapeptide in the brain and cognitive decline. JAMA 283, 1571–1577.

Ni, R., Marutle, A., Nordberg, A., 2013. Modulation of α7 nicotinic acetylcholine receptor and fibrillar amyloid-β interactions in Alzheimer's disease brain. J. Alzheimers Dis. 33, 841–851.

Oddo, S., Caccamo, A., Shepherd, J., Murphy, M., Golde, T., Kayed, R., Metherate, R., Mattson, M.P., Akbari, Y., LaFerla, F.M., 2003. Triple-transgenic model of Alzheimer's disease with plaques and tangles: intracellular Abeta and synaptic dysfunction. Neuron 39, 409–421.

Ondrejcak, T., Wang, Q., Kew, J., Virley, D., Upton, N., Anwyl, R., Rowan, M.J., 2012. Activation of α7 nicotinic acetylcholine receptors persistently enhances hippocampal synaptic transmission and prevents Aß-mediated inhibition of LTP in the rat hippocampus. Eur. J. Pharmacol. 677, 63–70.

Prince, M., Wimo, A., Guerchet, M., Ali, G.-C., Wu, Y.-T., Prina, M., 2015. World Alzheimer Report 2015. Alzheimer's Disease International, London.

Stoothoff, W., Johnson, G., 2005. Tau phosphorylation: physiological and pathological consequences. Biochim. Biophys. Acta 1739, 280–297.

Stucky, A., Bakshi, K., Friedman, E., Wang, H., 2016. Prenatal cocaine exposure upregulates BDNF-TrkB signaling. PLoS One 11, e0160585.

Tong, M., Arora, K., White, M., Nichols, R., 2011. Role of key aromatic residues in the ligand-binding domain of alpha7 nicotinic receptors in the agonist action of beta-amyloid. J. Biol. Chem. 286, 34373–34381.

Trojanowski, J., Vandeerstichele, H., Korecka, M., Clark, C., Aisen, P., Petersen, R., Blennow, K., Soares, H., Simon, A., Lewczuk, P., Dean, R., Siemers, E., Potter, W.Z., Weiner, M.W., Jack Jr, C.R., Jagust, W., Toga, A.W., Lee, V.M., Shaw, L.M., Alzheimer's Disease Neuroimaging Initiative, 2010. Update on the biomarker core of the Alzheimer's disease neuroimaging initiative subjects. Alzheimers Dement 6, 230–238.

Ui, N., 1973. Conformational studies on proteins by isoelectric focusing. Ann. N. Y Acad. Sci. 209, 198–209.
Um, J., Kaufman, A., Kostylev, M., Heiss, J., Stagi, M., Takahashi, H., Kerrisk, M.E., Vortmeyer, A., Wisniewski, T., Koleske, A.J., Gunther, E.C., Nygaard, H.B., Strittmatter, S.M., 2013. Metabotropic glutamate receptor 5 is a coreceptor for Alzheimer Aβ oligomer bound to cellular prion protein. Neuron 79, 887–902.
Wang, H.-Y., Bakshi, K., Frankfurt, M., Stuckey, A., Goberdhan, M., Shah, S., Burns, L.H., 2012. Reducing amyloid-related Alzheimer's disease pathogenesis by a small molecule targeting filamin A. J. Neurosci. 32, 9773–9784.
Wang, H.-Y., Bakshi, K., Shen, C., Frankfurt, M., Trocme-Thibierge, C., M, P., 2010. S 24795 limits β-amyloid - α7 nicotinic receptor interaction and reduces Alzheimer's disease-like pathologies. Biol. Psychiatry 67, 522–530.
Wang, H.-Y., Frankfurt, M., Burns, L.H., 2008. High-affinity naloxone binding to filamin A prevents mu opioid receptor - Gs coupling underlying opioid tolerance and dependence. PLoS One 3, e1554.
Wang, H.-Y., Lee, D., D'Andrea, M., Peterson, P., Shank, R., Reitz, A., 2000a. beta-amyloid(1-42) binds to alpha7 nicotinic acetylcholine receptor with high affinity. Implications for Alzheimer's disease pathology. J. Biol. Chem. 275, 5626–5632.
Wang, H.-Y., Lee, D., Davis, C., Shank, R., 2000b. Amyloid peptide Abeta(1-42) binds selectively and with picomolar affinity to alpha7 nicotinic acetylcholine receptors. J. Neurochem. 75, 1155–1161.
Wang, H.-Y., Li, W., Benedetti, N., Lee, D., 2003. α7 Nicotinic acetylcholine receptors mediate β-amyloid peptide-induced tau protein phosphorylation. J. Biol. Chem. 278, 31547–31553.
Wang, J., Xia, Y., Grundke-Iqbal, I., Iqbal, K., 2013. Abnormal hyperphosphorylation of tau: sites, regulation, and molecular mechanism of neurofibrillary degeneration. J. Alzheimers Dis. 33 (Suppl 1), S123–S139.
Wesierska, M., Dockery, C., Fenton, A., 2005. Beyond memory, navigation, and inhibition: behavioral evidence for hippocampus-dependent cognitive coordination in the rat. J. Neurosci. 25, 2413–2419.
Wesson, D., Wilson, D., 2011. Age and gene overexpression interact to abolish nesting behavior in Tg2576 amyloid precursor protein (APP) mice. Bev. Brain Neurosci. 216, 408–413.
Yamamoto, T., Hirano, A., 1986. A comparative study of modified Bielschowsky, Bodian and thioflavin S stains on Alzheimer's neurofibrillary tangles. Neuropathol. Appl. Neurobiol. 12, 3–9.
Yau, J., McNair, K., Noble, J., Brownstein, D., Hibberd, C., Morton, N., Mullins, J.J., Morris, R.G., Cobb, S., Seckl, J.R., 2007. Enhanced hippocampal long-term potentiation and spatial learning in aged 11ß-hydroxysteroid dehydrogenase type 1 knock-out mice. J. Neurosci. 27, 10487–10496.
Zhang, L., Xie, J., Yang, J., Cao, Y., 2013. Tyrosine phosphatase STEP61 negatively regulates amyloid β-mediated ERK/CREB signaling pathways via α7 nicotinic acetylcholine receptors. J. Neurosci. Res. 91, 1581–1590.